Carbon monoxide poisoning and mitigation strategies for polymer electrolyte membrane fuel cells – A review

Velia Fabiola Valdes-Lopez[1], Tom Mason[1], Paul R. Shearing[1], Dan J. L. Brett[1*]

[1]Electrochemical Innovation Lab, Department of Chemical Engineering, University College London, Torrington Place, WC1E 7JE, London, UK

Abstract

Polymer electrolyte membrane fuel cells (PEMFC) have received much attention due to their high power density, good start-stop capabilities and high gravimetric and volumetric power density compared with other fuel cells. However, certain technological challenges persist, which include the fact that conventional anode electrocatalysts are poisoned by low levels (few ppm) of carbon monoxide (CO). This review considers the mechanism of CO poisoning and the effects that it has on the PEMFC performance. The key parameters affecting CO poisoning are identified and methods used to mitigate the effects are discussed. These mitigation strategies are divided into three groups according to the means by which the technologies are applied: pre-treatment of reformate, on board removal of CO and *in operando* mitigation strategies.

Keywords

PEMFC; CO poisoning; mechanisms; catalysts; diagnostics; hydrogen separation and purification; mitigation strategies

Contents

[*]*Corresponding author.* Tel.: +44(0)20 7679 3310.

Email: d.brett@ucl.ac.uk

1. Introduction

Fuel cells are considered a highly efficient energy source, with the advantage of no carbon dioxide emissions at the point of use, when operating on hydrogen fuel. They can contribute to meeting global energy demands while overcoming environmental challenges. They could potentially replace internal combustion engines, and in some cases energy storage devices such as batteries.[1] Polymer electrolyte membrane fuel cells (PEMFCs) in particular have received much attention as they have high power density and fast start-up and response times.[2] For these reasons, they are the most commonly used fuel cell for automotive applications.[3, 4] In 2017, PEMFCs accounted for 75% of the total megawatts.[5]

The most important challenges that this technology faces in order to increase its presence in the market are cost, performance and durability.[6] A range of physical-chemical phenomena can adversely affect performance, including water management issues (membrane humidification, cathode flooding, freezing, drying phenomena), adsorption of contaminants, degradation and poisoning of electrocatalysts, etc. Some of these processes are reversible, others are irreversible and lead to long-term degradation.[7] Contaminants such as carbon monoxide (CO), hydrogen sulphide (H_2S) and ammonia (NH_3)[8] are known to be particularly pernicious and affect performance, even when present in trace (ppm) amounts.[9] This work focuses on the effect of carbon monoxide on PEMFCs, which is usually introduced by the hydrogen fuel supply. The International Organization for Standardization (ISO) state that the limits for vehicle and stationary applications are 0.2 and 10 ppm CO respectively[10, 11] but methods of mitigating CO poisoning can potentially allow practical operation at higher levels. The purpose of this review is to provide a general overview of the studies that have looked at the mechanism of CO poisoning and in particular, to examine the mitigation strategies proposed.

2. Fundamental understanding

2.1 Hydrogen quality for PEMFC

Around 48% of worldwide hydrogen production comes from steam methane reforming (SMR) of natural gas, or other hydrocarbons [12]. This process delivers high conversion to hydrogen at a low cost and high efficiency. Other mature and commercialized technologies are auto-thermal reforming (ATR) of methane and coal gasification. Some predictions expect this to be the most economical path to hydrogen production for decades to come.[13] While this may be a convenient and economical route, the hydrogen produces is not necessarily conducive to direct use in PEMFC. The reformate obtained after a first stage of clean-up through the water-gas-shift (WGS) reaction, has a typical composition of 40 to 70% H_2, 15 to 25% CO_2, 1 to 2% CO, plus small quantities of inert gases such as water vapour and nitrogen, and sulphur impurities. It is also possible to find ammonia in the reformate at ppm levels, if it is used as a gas tracer along the distribution system.[14]

Multiple purification stages are needed to reduce the CO concentration to levels conducive to PEMFC operation after the generation of hydrogen from fossil fuels. Typically, the concentration of CO obtained after these processes is of the order of 10 ppm. Purification methods include adsorption, membrane separation, scrubbers, and selective reaction. Pressure swing adsorption (PSA) is the most common technology, accounting for 85% of the hydrogen purified.[13] CO preferential oxidation (PROX) and the CO-selective methanation (SMET) are receiving increasing interest and will be discussed in Section 2.1.[15] These clean-up stages can require an order of magnitude higher plant volume than that for the reformer and fuel cell stack combined,[16] increasing the costs and parasitic power demand. It has been estimated that in large-scale chemical plants, separation and purification of hydrogen can account for between 50 and 80% of the total capital investment.[17] The deployment of fuel cells is hindered as a consequence.[18]

The reformation of liquid and renewable biomass materials, such as methanol and ethanol, is being studied as an alternative to natural gas, especially due to the advantage of liquid storage and transport compared to gases.[19, 20] Electrolysis of water is being extensively developed as a route to hydrogen from 'green' electricity.[12] Other sources include photosynthetic microorganisms, the photoelectrolysis of water, the thermal dissociation of water and thermochemical cycles.[21]

2.2 Mechanisms of CO poisoning

2.2.1 Electrochemical reactions in a PEMFC

Figure 1 summarises the key components of a PEMFC along with the action of CO in the fuel stream on a conventional (e.g. Pt) catalyst. The hydrogen oxidation reaction (HOR) takes place at the anode through the Tafel,[22] Heyrovsky[23] and Volmer[24] mechanisms. The HOR usually takes place through the Tafel-Volmer, and/or the Heyrovsky-Volmer routes,[25] although alternative routes are under study.[26]

In the early studies about HOR, it was reported that the reaction was insensitive to surface structure.[27] More recently, it was found that the reaction rate is dependent on the surface structure and the electrolyte.[28, 29] For the most common anode catalyst, platinum, the rate of hydrogen oxidation depends on the crystal orientation following the trend Pt(110)>Pt(100)>Pt(111). The Tafel reaction is the rate-limiting step in the case of Pt(110):[30, 31]

$$\mathbf{2Pt + H_2 \leftrightarrow 2Pt - 2H_{ads}} \quad \text{(Tafel reaction)} \quad (1)$$

$$\mathbf{Pt + H_2 \leftrightarrow Pt - H_{ads} + H^+ + e^-} \quad \text{(Heyrovski reaction)} \quad (2)$$

$$\mathbf{2Pt - H_{ads} \leftrightarrow 2Pt + 2H^+ + 2e^-} \quad \text{(Volmer reaction)} \quad (3)$$

CO competes with hydrogen for the active sites on the platinum under normal anode operating potentials.[32] CO adsorbs on the Pt surface more easily than H_2 (heat of adsorption of CO on Pt is 134 kJ mol^{-1}, and for H_2 is 87.9 kJ mol^{-1}).[33] The

available surface for the HOR is reduced while the CO accumulates on the platinum surface.[34] The magnitude of the surface covered by CO is determined by the CO adsorption and/or re-adsorption (Reactions 4 and 5),[35] the electroreduction of CO_2, and the CO removal through oxidation (Reaction 6), which occurs through the reactant pair mechanism. [36] These processes compete with each other, depending on conditions.[37]

$$\mathbf{CO + nPt \leftrightarrow Pt_n - CO_{ads}} \quad (4)$$

$$\mathbf{2CO + 2(Pt - H_{ads}) \leftrightarrow 2(Pt - CO_{ads}) + H_2} \quad (5)$$

$$\mathbf{Pt - CO_{ads} + Pt - H_2O_{ads} \leftrightarrow 2Pt + CO_2 + 2H^+ + 2e^-} \quad (6)$$

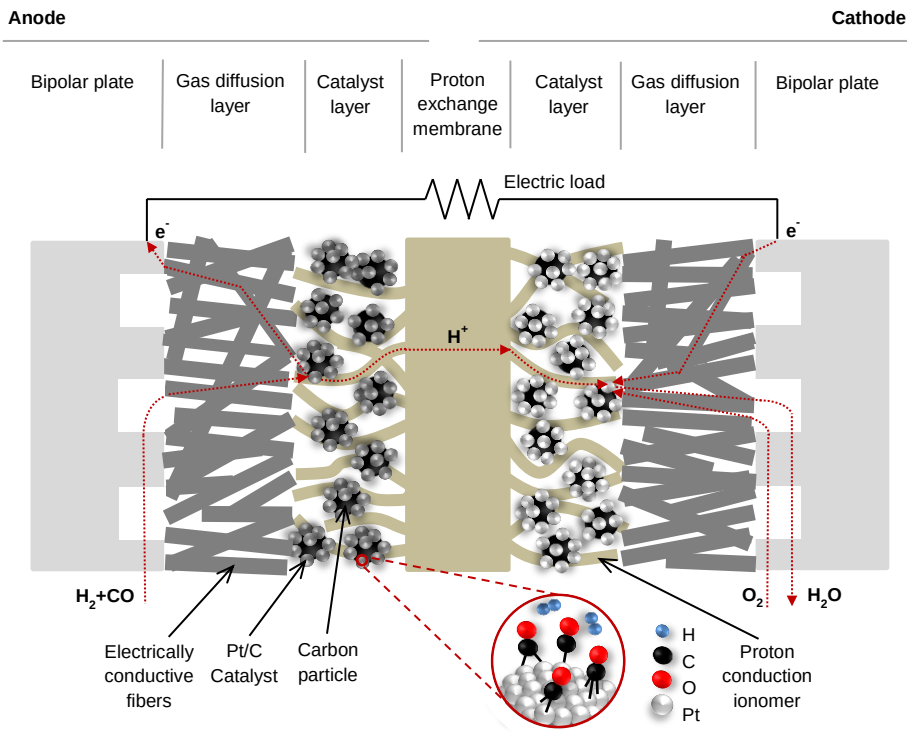

Figure 1: Diagram showing the key components of the PEMFC along with the action of CO in the hydrogen feed on the anode catalyst.

Figure 1 also shows that different adsorption modes exist for CO on Pt: linear or on-top bonding, bridge or twofold site bonding and hollow or threefold site bonding. The type of CO adsorption site bonding is related to the surface structure at saturation coverage.[29] It has been shown that at less than 50% surface coverage, the bridge-bonded dominates. The linear bonded type is dominant at higher surface coverage (Figure 2).[38]

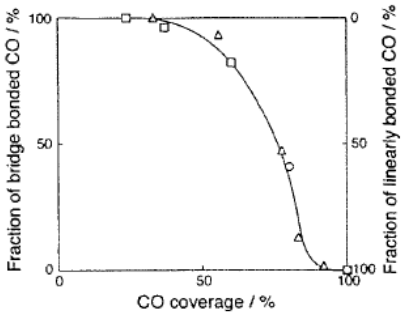

Figure 2: Proportion of bridged-bonded or linearly bonded CO sites on Pt at different CO concentrations (O) 10 ppm; (□) 20 ppm; (Δ) 40 ppm; (●) 100 ppm. Reproduced with permission.[38] Copyright 1995, Elsevier.

The increasing coverage of CO on the platinum surface reaches a threshold where the electro-oxidation of CO takes place. For pure platinum electrodes, it takes place above ≈ 0.6 V (vs. RHE).[39] At 25 °C, the CO contained in 1% CO/hydrogen mixture blocks 98% of the active sites.[40] Figure 3 presents the cyclic voltammograms obtained for the CO stripping on a Pt/C catalyst at 23 °C.[37]

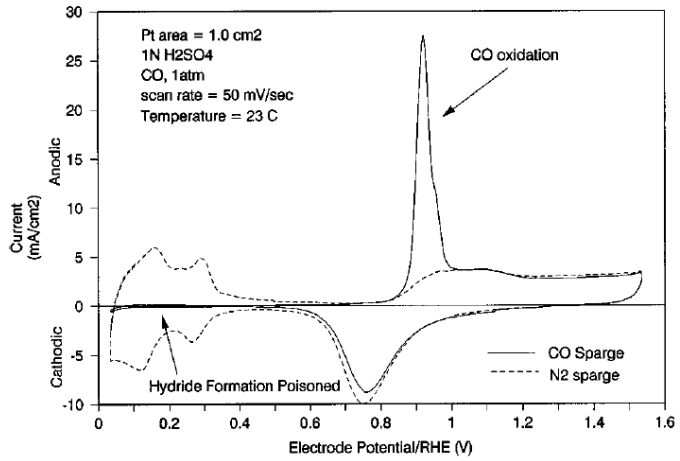

Figure 3: Cyclic voltammograms obtained on polycrystalline Pt at 23 °C in the presence and absence of CO. Reproduced with permission.[37] Copyright 1996, American Chemical Society.

2.2.2 "Self-oxidation" or sustained potential oscillations

Murthy *et al*. (2001) first reported the oscillatory behaviour of the potential in an operando cell exposed to CO/H_2 at a constant current.[41] Zhang and Datta (2002) subsequently reported more details about this behaviour.[42, 43] These oscillations were also presented by Hanke-Rauschenbach *et al.* (2011) as part of a review of nonlinear dynamics of fuel cells.[44] As the CO accumulates at the surface of the catalyst, the anodic overpotential increases. The higher potential attained allows the oxidation of the CO (as shown in Figure 3), and the cell voltage increases (anode overpotential

decreases) to the original value,[45] with the process of CO build-up occurring again, this cycle leading to anode overpotential oscillations, as shown in Figure 4 for different operating conditions.

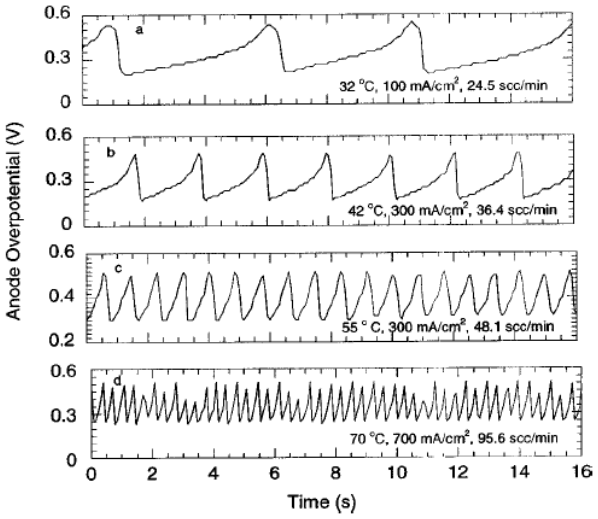

Figure 4. Anode overpotential oscillations caused by exposure to CO/H_2 in a PtRu/C anode catalyst. The operating conditions of cell temperature, current density, and anode inlet flow rate are: a) 32°C, 100 mA cm^{-2}, 24.5 sccm; b) 42°C, 300 mA cm^{-2}, 36.4 sccm; c) 55°C, 300 mA cm^{-2}, 48.1 sccm; d) 70°C, 700 mA cm^{-2}, 95.6 sccm. Reproduced with permission [42]. Copyright 2002, The Electrochemical Society, Inc.

This behaviour was first observed in PtRu/C,[41-43] Pd-Pt/C and Pd/C[46] before being studied in Pt/C systems.[47] The nature of the oscillations depends on the temperature, current density, anode CO concentration and flow rate. Generally, the higher the concentration of CO and anodic flow rate are, the shorter the periods are. The period decreases with increasing current density or temperature.[42, 48]

The dynamics of the oscillations were studied by Mota *et al*. (2010) at different current and anode flow rates, observing periodic and nonperiodic states. The transition from 'period-1' to 'period-2' and chaotic states occurs with an increase in current at a fixed flow, or over the decrease of the flow rate at a constant current.[49] This behaviour was corroborated in spatio-temporal models[50, 51] and current distribution measurements.[52]

Lu *et al*. (2011) determined that the time-averaged power density obtained with self-sustained oscillations under galvanostatic operation is higher than when in potentiostatic mode. The measurement of the concentration of CO at the anode outlet under constant current contributed to confirm the electrochemical oxidation of CO, which is responsible for the difference in the power output between the two operation modes.[48] Subsequently, Lopes *et al*. (2013) showed the production of CO_2 during the oscillatory behaviour, and presented a model that predicts the coverage of the different species in the electrode surface.[53]

2.3 Effects of CO on the performance of PEMFCs

2.3.1 Effect of operating parameters

CO poisoning affects PEM fuel cell performance in three major ways: the electrode kinetics, conductivity and mass transfer.[14] Blocking of catalyst active sites affects the kinetics of electrocatalysis.[33] Figure 5 summarises the effects of concentration, exposure time, temperature, anode flow rate and operating pressure, from a range of experimental investigations.

Early studies show that the effect of CO becomes more severe on Pt electrocatalysts when the CO concentration and time are increased.[54-56] At higher concentrations (typically higher than 100 ppm CO), two slopes are observed in the polarization curves. The slope at lower current densities is due to the adsorption and oxidation of hydrogen and CO at the anode. At higher current densities, the potential at the anode reaches values at which the adsorbed CO is oxidized to CO_2 and the reaction rates for hydrogen adsorption and oxidation are increased.[54] Over time, as the adsorption of CO increases, the performance decreases significantly until it reaches a steady state.[54, 57]

Temperature has a strong impact on the effect of CO poisoning. The adsorption of CO is favoured at lower temperatures, blocking the oxidation of H_2.[58] Zamel *et al.* reported that at higher temperatures the poisoning occurs faster, resulting in a more rapid performance drop towards the steady state.[59] Dhar *et al*. (1987) found that the CO coverage follows a Temkin isotherm at a fixed current density, which can be written in the form:[58]

$$\boldsymbol{\theta_{CO} = \frac{-\Delta Go^{\circ}}{r} - \frac{RT}{r}\ln H + \frac{RT}{r}\ln\left(\frac{[CO]}{[H_2]}\right)} \quad (1)$$

Where θ_{CO} is the CO coverage, ΔG_o^0 is the standard free energy of adsorption, r is the interaction parameter, and H Henry's law constant for CO solubility (atm L mol^{-1}). This relation shows that the increase in the anodic polarization is due to the replacement of H_2 molecules by CO. The interaction parameter is highly dependent on the catalyst structure.[58] As the anode flow is increased, the voltage of the cell decreases due to the increased total amount of CO that is exposed to the anode. Additionally, the time needed to reach steady-state is diminished as the flow rate is increased.

Another important operating parameter is the cathode pressure. Oxygen permeates through the membrane from the cathode to anode and contributes to the oxidation of the CO into CO_2.[60] Figure 5(e) shows the combined effect of the concentration of CO and the operating pressure.[61]

The influence of the anode feed relative humidity has also been studied. Iorio *et al*. (2002) determined that the CO-stripping potential of Pt/C and PtRu/C electrodes decreased at higher water vapor pressure.[62] In high-temperature PEMFCs (HT-PEMFCs), an increase in the humidity reduces the anodic overpotential. This is due to the presence of the OH_{ads} groups, which are consumed in the oxidation of CO (Figure 4(f)).[63-65]

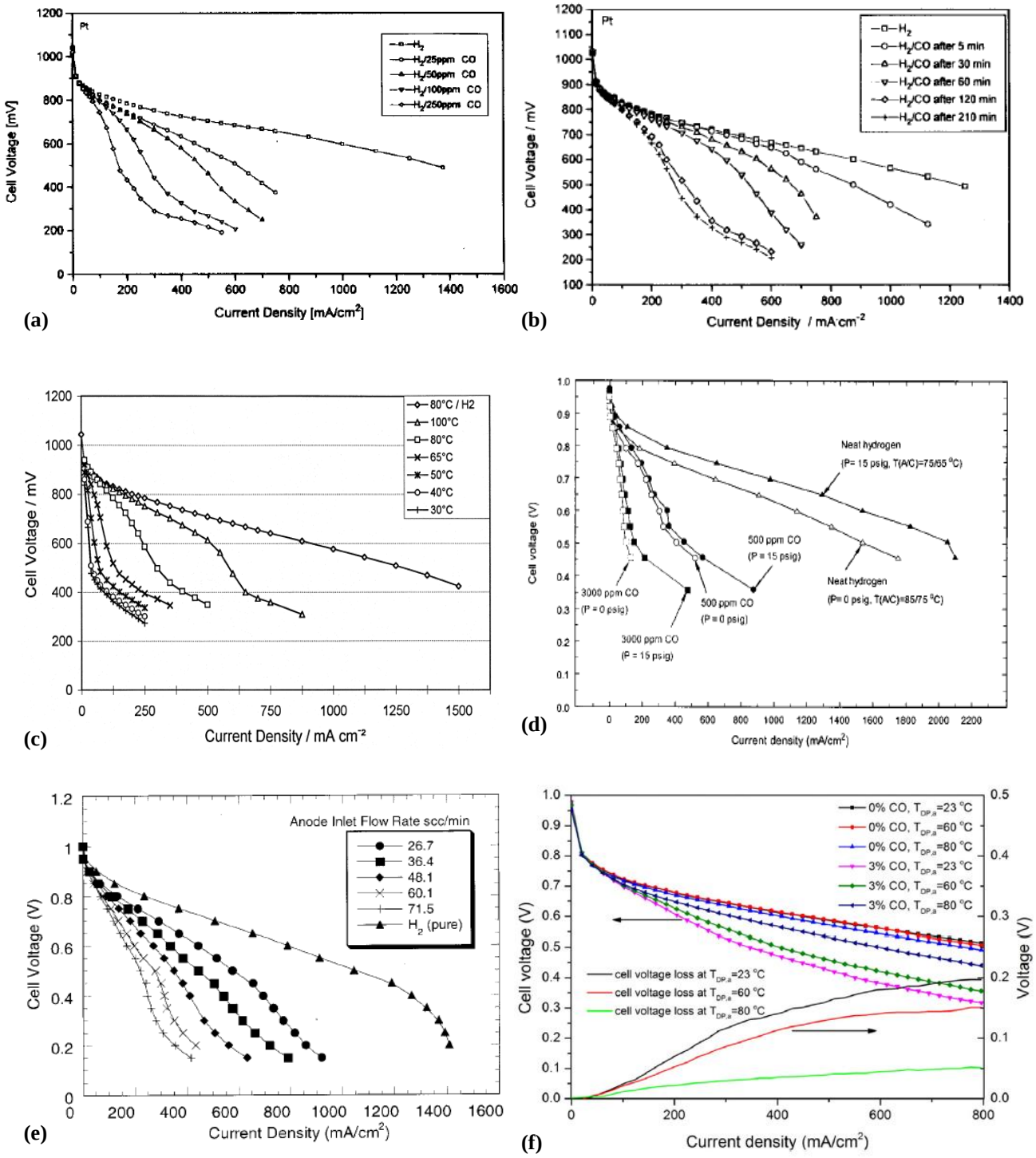

Figure 5: Operating parameters that influence the performance of PEMFC in the presence of CO in the anode inlet. (a) Effect of the concentration of CO (ppm). Reproduced with permission.[54] Copyright 1996, The Electrochemical Society, Inc. (b) Effect of the exposure time with 100 ppm CO/ H_2//O_2. Reproduced with permission.[54] Copyright 1996, The Electrochemical Society, Inc. (c) Effect of the temperature. Reproduced with permission.[66] Copyright, 1998, Elsevier. (d) Effect of the pressure and concentration of CO. Reproduced with permission.[61] Copyright 2003, The Electrochemical Society, Inc. (e) Effect of the anode flow over the exposure to 108 ppm CO/H_2. Reproduced with permission.[60] Copyright 2002, The Electrochemical Society, Inc. (f) Effect of the anode dew point temperatures in HT-PEMFC. Reproduced with permission.[63] Copyright 2015, Elsevier

2.3.2 Influence of additional contaminants

2.3.2.1 The combined effect of CO and CO_2

The presence of CO_2 in the anode inlet is closely related to the CO poisoning, as the reverse water-shift reaction (RWGS) produces CO in the presence of platinum.[37, 65, 67-70] 100-200 ppm CO can be reached with a 75% H_2/25% CO_2 feed:[37]

$$\boldsymbol{2Pt + H_2 \rightarrow 2Pt - 2H} \quad (7)$$

$$\boldsymbol{CO_2 + 2Pt - H \rightarrow Pt - CO + H_2O + Pt} \quad (8)$$

Due to the endothermic nature of the RWGS, the production of CO is increased at higher temperatures.[63, 67] As incrementing the temperature also favours the CO electro-oxidation, the degradation of cells is determined by the ratio: $CO_{production}/CO_{electro\text{-}oxidation}$, HT-PEMFCs are particularly sensitive to this.[65] The humidity also has a direct impact on RWGS CO_2 poisoning, as at higher water content the CO produced is oxidised through the water gas shift reaction.[63, 65, 67]

The combined effect of CO and CO_2 in the anode inlet has been studied. As the adsorption of CO is much faster than the RWGS, the polarization due to the presence of CO in the anode inlet is higher than for CO_2. This distinction is more evident at high concentrations of CO, as less Pt-H sites are available for the RWGS reaction to take place.[37, 67, 71] Figure 6 shows the combined effect of CO and CO_2 on an HT-PEMFC.[63]

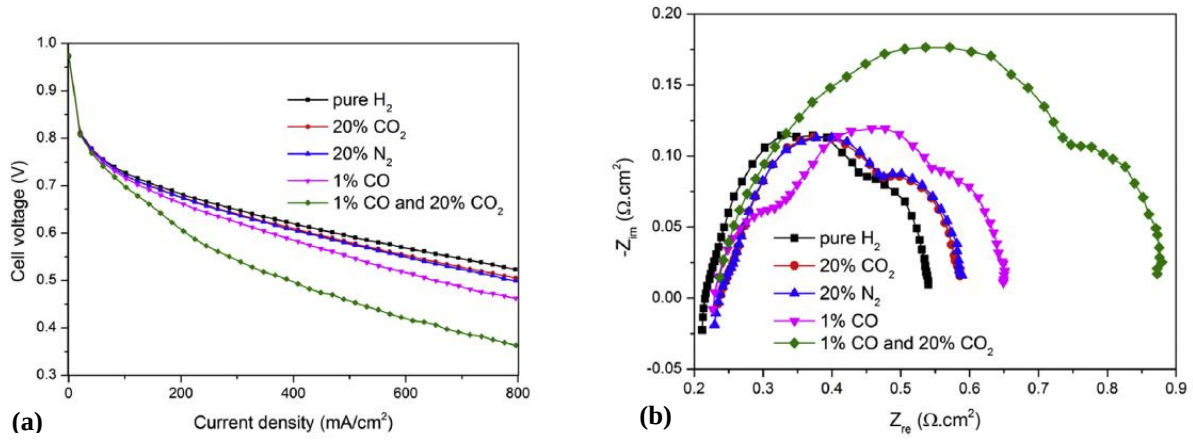

Figure 6. Effects of 1% CO, 20% CO_2 and a mixture of both contaminants on the operation of a high-temperature fuel cell, compared with the injection of 20% N_2: (a) polarization curves, and (b) galvanostatic electrochemical impedance spectra. Reproduced with permission.[63] Copyright 2015, Elsevier.

2.3.2.2 The combined effect of CO and H_2S

Rockward *et al.* (2007) presented the contamination of multiple components in a PEMFC. The combination of H_2S and CO, in particular, was studied through cyclic voltammetry. It was observed that in the presence of both components, the CO is displaced from the surface (Figure 7). The longer the exposure time, the more the CO is displaced and the H_2S is adsorbed.[72] This phenomenon could be explained by the H_2S affinity for platinum, which is higher than for CO. S-species are a common component in the reformate, capable of irreversible effects in the cells.[73]

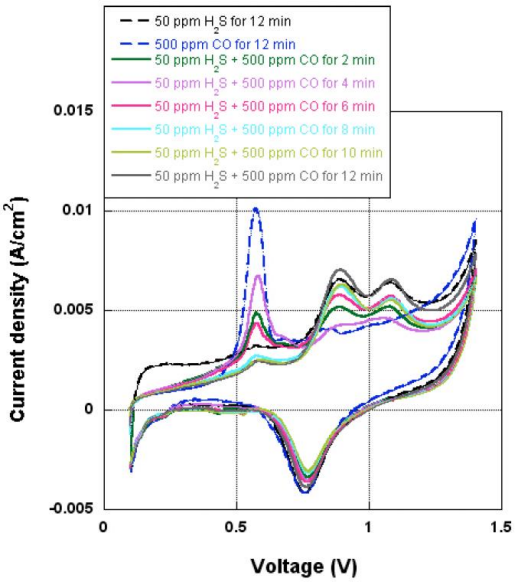

Figure 7. Cyclic voltammograms obtained for exposure to 500 ppm CO and 50 ppm H_2S at 2, 4, 5, 8, 10 and 12 minutes, showing the displacement of CO in the presence of H_2S. Reproduced with permission.[72] Copyright 2007, The Electrochemical Society, Inc.

2.3.2.3 The combined effect of CO, H_2S, formic acid, benzene and ammonia

Wang *et al.* (2014) evaluated the additive effect of other common impurities in hydrogen. The effect of 0.2 ppm CO, 4 ppb H_2S, 0.2 ppm formic acid, 2 ppm benzene and 0.1 ppm ammonia on hydrogen was evaluated individually, without any significant effect on the performance of the cell. The mixture did not have a major impact either. However, when the concentration of the contaminants was increased five times, the effects were discernible (

Figure 8). Subsequently, cell performance almost fully recovered, but a permanent degradation of the membrane was observed.[74]

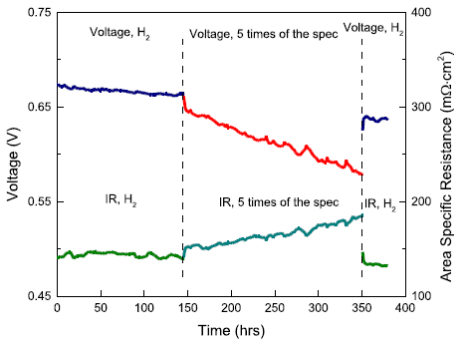

Figure 8. Effect of a mixture comprising 1 ppm CO, 20 ppb H_2S, 1 ppm formic acid, 10 ppm benzene and 0.5 ppm ammonia in hydrogen on the voltage of a cell operated galvanostatically at 1000 mA cm^{-2}. Reproduced with permission.[75] Copyright 2014, Elsevier.

2.3.2.4 The combined effect of CO and toluene

Toluene (C_7H_8) is an aromatic hydrocarbon, also present in the reformate.[74, 76, 77] The effects of single-component C_7H_8 and CO, and mixtures thereof, have been studied.[77-79] Concentrations of 2 ppm or 20 ppm C_7H_8 did not have a significant effect on the performance of the cell due to its hydrogenation to methylcyclohexane (C_7H_{14}).[77, 78] The effects of a mixture of 2 ppm C_7H_8 with 0.2 ppm CO had the same effects than the CO alone.[78] However, when 20 ppm C_7H_8 was mixed with 2 ppm CO, the resultant overpotential increased to higher values than the sum of the individual contributions (Figure 9). As the CO is adsorbed on the surface, the HOR and C_7H_8 hydrogenation compete for the active sites, hampering the fuel cell performance.[77] Angelo *et al.* (2010) subsequently evaluated the effects of a mixture containing 0.2 ppm CO and 2 ppm C_7H_{14}. It was found that the effects on the performance were similar to the exposure of CO alone.[78]

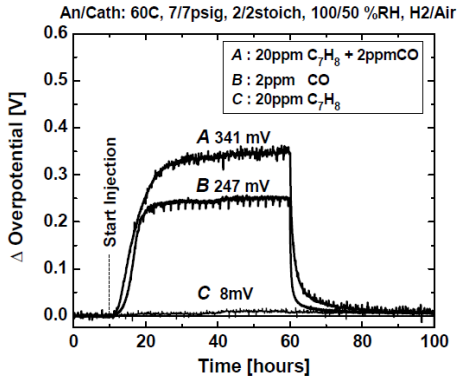

Figure 9. Comparison of the cell overpotentials resulting from exposure to 20 ppm C_7H_8, 2 ppm CO and a mixture containing 20 ppm C_7H_8 and 2 ppm CO under galvanostatic control at 1 A cm^{-2} (60 °C). Reproduced with permission.[77] Copyright 2008, The Electrochemical Society, Inc.

2.4 Contamination of the cathode

In the presence of CO at the anode, it can pass through the membrane and be absorbed on the cathode catalyst, especially on the sites closer to the membrane. Cyclic voltammetry was used to prove the presence of CO on the cathode. The potentials of both electrodes are affected simultaneously (Figure 10). Different parameters affect the CO crossover, including the porosity, levels of humidification and the thickness of the membrane, and the pressure difference between anode and cathode. A fully hydrated membrane reduces CO crossover.[80, 81]

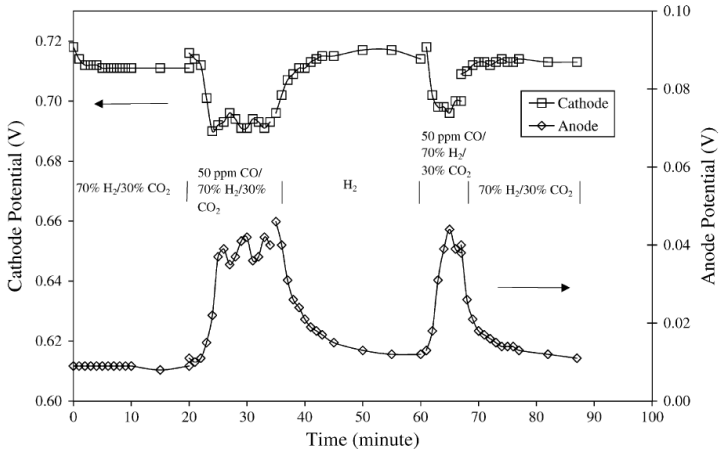

Figure 10 Evolution of the anode and cathode potentials over time in a PEMFC operated at 300 mA cm^{-2} with different compositions of anode fuel. Anode: Pt-Ru (0.62 mg cm^{-2}), and cathode: Pt (1.8 mg cm^{-2}). Reproduced with permission.[81] Copyright 2002, Elsevier.

Reshetenko *et al.* (2012) presented the study of a segmented cell exposed to 2 ppm CO/H_2 in H_2/O_2, H_2/air and H_2/H_2 systems under galvanostatic mode at various current densities up to 1.4 A cm^{-2}. Both electrodes showed a drop in the ECSA.[82, 83] The active area loss in both electrodes has been confirmed in long-term (about 1000 hour) experiments under cyclic exposure to CO,[84] and under different load cycling protocols[85] (Section 1.5).

Wagner *et al.* (2004) studied the poisoning of CO through electrochemical impedance spectroscopy, and showed an increase on both electrodes at constant cell voltage. At constant current, the increase on the impedance resulted mainly by the anode contribution.[86] This information was complemented by the spatial electrochemical impedance spectroscopy results, where the increase on both electrodes was observed at constant current in the presence of 2 ppm CO (Section 1.6.3).[82, 83]

Other studies have focused on the effect of CO in the anode, on the corrosion of carbon supports in the cathode. Parry *et el.* (2011) shown through XPS a decrease in the corrosion of the carbon catalyst-support in the cathode in the presence of 5 ppm CO in the anode. This effect was explained by the reduction of the reverse proton pumping from the cathode to the anode.[33, 87] In an HT-PEMFC, CO in the range of 0.1-1.3% was added directly to the cathode to evaluate the corrosion rate of carbon-supports. A competition between CO, O_2 and H_3PO_4 at the three-phase boundaries was shown. The H_3PO_4

molecules that hamper the performance of the cell, are replaced by CO. Hence, a low CO content in the cathode side increases the cell potential. Higher concentrations of CO are detrimental due to extensive blockage of the active sites.[88]

2.5 Long-term studies

Fewer studies have considered the long-term degradation of PEM fuel cells when exposed to CO. Angelo *et al.* (2008) reported the loss in the active area of both electrodes over 1000 hours with repetitive exposure to 2 ppm CO, showing the negative impacts of CO in the performance and durability of the cell (Figure 11).[84] Profatilova *et al.* (2018) studied load cycling protocols in the presence of CO for about 1000 hours, and confirmed the irreversible losses in the active surface of the electrodes. The main accelerating aging parameters were also identified, which include the CO concentration, the amplitude and frequency of current load cycling, and the application of intermediate electrochemical in situ characterizations.[85]

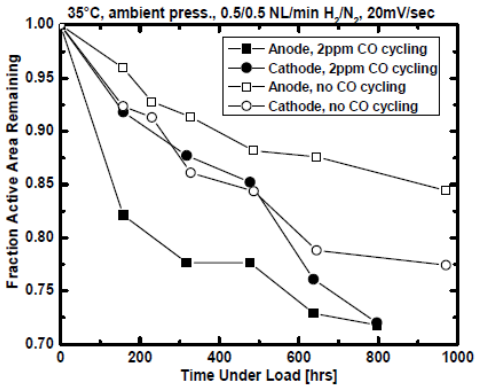

Figure 11. Evolution of active area loss in the anode and cathode over long term operation under repetitive exposure to 2 ppm CO. Reproduced with permission.[84] Copyright 2008, The Electrochemical Society, Inc.

Franco *et al.* (2009) examined the effects of 5 ppm CO on an MEA after 600 h under two different current-cycle protocols, representative of transport applications:

- Protocol $0/I_{max}$: alternation of 30 min at 0 A cm^{-2} and 30 min at 0.54 A cm^{-2}
- Protocol I_{min}/I_{max}: alternation of 30 min at 0.108 A cm^{-2} and 30 min at 0.54 A cm^{-2}

Figure 12 presents the results of both tests. It was found that the current-cycle operating conditions are strongly related to the effects of CO on the cell potential degradation rate. Under the $0/I_{max}$ protocol, the performance of the cell is degraded in the presence of CO in the short and long-term, mainly because of the contamination of CO that blocked the anode catalytic sites. It is not the case for the long-term degradation under I_{min}/I_{max}, where it is lower under H_2+CO than with pure H_2. As the fuel starvation is higher under the I_{min}/I_{max} protocol, the concentration of the permeated O_2 in the anode is accumulated. The O_2 reacts with the CO, reducing both the poisoning and the carbon-support corrosion on the cathode.

The corrosion decreases the cathode thickness and the catalyst active surface area, degrading the performance of the cell. Thus, the CO poisoning in the anode can be used as a tool to mitigate the cathode catalyst-support corrosion and increase the durability of the MEA.[89] The finding was confirmed through XPS quantitative characterizations by Parry *et al.* (2011), that observed the decrease of the reverse proton pumping effect between the cathode and the anode in the presence of CO.[87]

More recently, Chandesris *et al.* (2018) studied the degradation heterogeneities in a stack exposed to reformate. It was found that the cathode outlet aged more severely than the inlet, and that the anode outlet would lose more CO tolerance.[90]

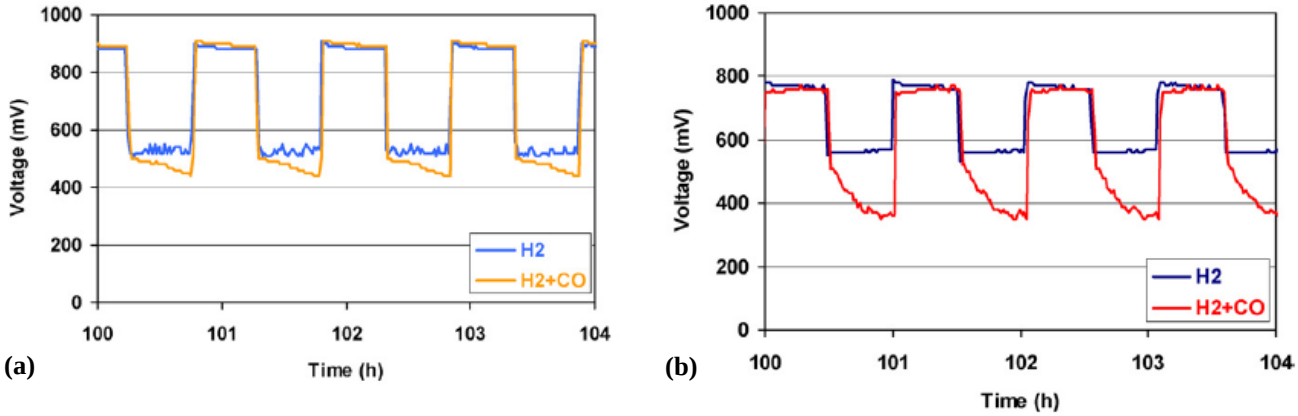

Figure 12.Long-term effect of H_2 and 5 ppm CO/H_2 for $0/I_{max}$ (a) and I_{min}/I_{max} (b) current-cycle protocols after 100 hours of operation. Reproduced with permission.[89] Copyright 2009, Elsevier.

2.6 Spatial distribution of the CO adsorption

2.6.1 Distribution in a single channel

The distribution 'pattern' of CO poisoning across the extent of the anode was studied by Brett *et al.* (2004). Localised CO stripping and adsorption transients were used to determine the distribution of CO to either side of a single linear flow channel (Figure 7). Low flow rates result in anisotropic distributions of CO away from the channel, and higher flows present a more uniform distribution. The advection along the channel and the lateral diffusion compete between each other. The dispersion of CO is a result of these two mechanisms.[91] The results obtained in this study helped to develop a model able to predict the effects of transient poisoning, which are present, in particular, during the system start-up, in the distribution of the CO adsorption. A good agreement with the experimental results was observed.[92]

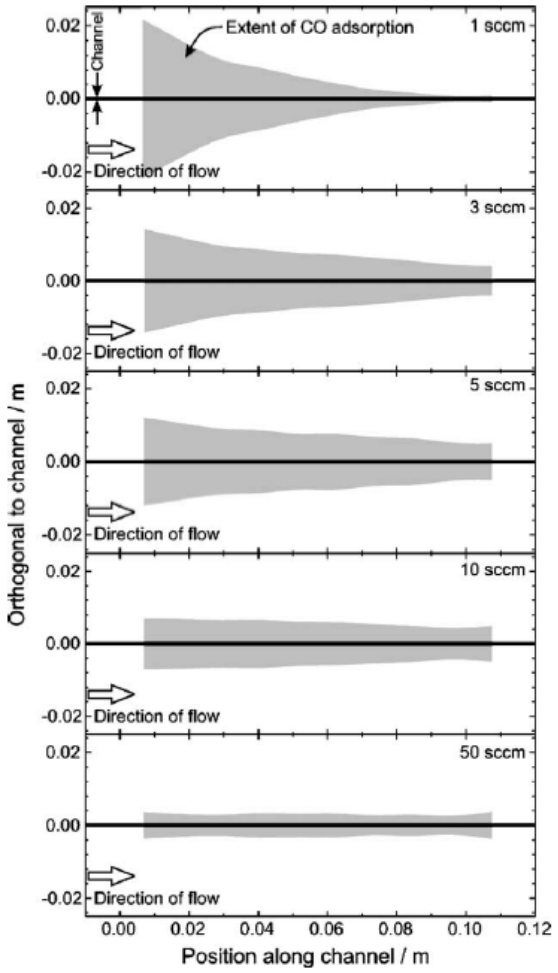

Figure 13: Distribution of the CO adsorption in a single cell at different flow rates of N_2, and a constant CO dose of 0.2 cm^3. Reproduced with permission.[91] Copyright 2004, Elsevier.

2.6.2 Current density distribution

Different authors proposed the use of segmented cells to evaluate the current distribution across a cell and assess the effect of CO poisoning.[70, 82, 83, 93, 94] It was found that under galvanostatic control and in the absence of self-sustained potential oscillations (usually low concentrations of CO), the distribution of the surface coverage by CO was uneven as the adsorption of CO is faster at the inlet than at the outlet (Figure 14 (a)).[82, 83, 93, 94] In the presence of potential oscillations, where the hydroxides formed at the surface of the catalyst assist the CO oxidation, the effects of the otherwise uneven distribution are diminished (Figure 14 (b)).[70] In potentiostatic mode, the anodic potential is maintained below the CO oxidation potential so that no substantial CO removal takes place.[70] More research is needed to understand the mechanisms occurring under potentiostatic control as Tingelof *et al.* reported an uneven distribution of the poisoning,[70] contrary to Boaventura *et al.* that described an even distribution.[94]

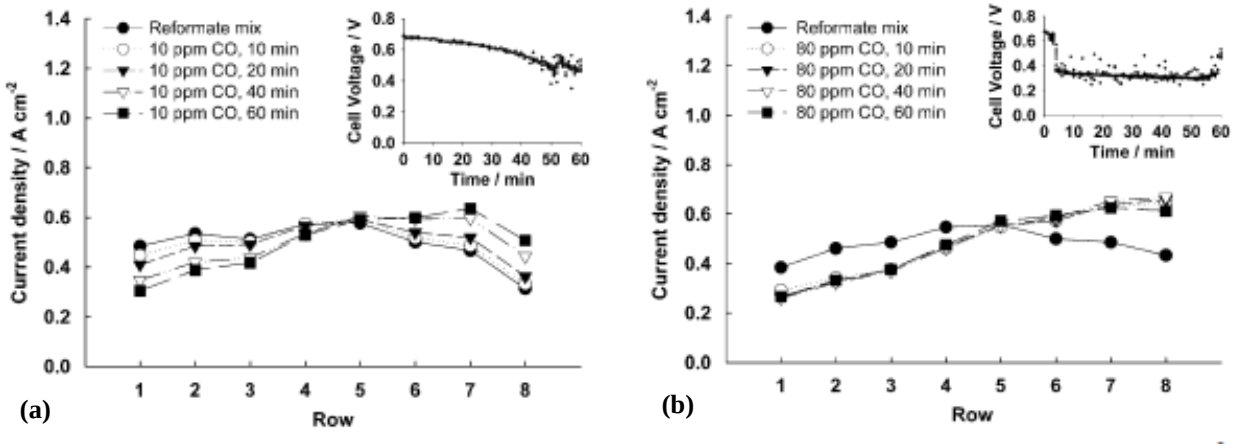

Figure 14. Current distribution transient behaviour of a cell (Pt/C) operating under galvanostatic control (0.5 A cm^{-2}) exposed to a simulated reformate gas mixture containing (a) 10 ppm CO, 50% H_2, 40% CO_2 and 10% N_2 and (b) 80 ppm CO, 50% H_2, 40% CO_2 and 10% N_2. Reproduced with permission.[70] Copyright 2008, Elsevier.

2.6.3 Segmented electrochemical impedance spectroscopy (EIS)

Electrochemical impedance spectroscopy (EIS) has been used to evaluate the progress of the CO poisoning. It constitutes an effective diagnostic technique to identify the contamination and to study the mechanisms involved in it.[95, 96] Considering the changing nature of the contamination over time, new methods for the interpretation have been developed. These techniques include real-time drift compensation, time course interpolation and Z-HIT refinement.[86, 97] During the contamination, an increase in the total impedance of the fuel cell is observed. In the case of galvanostatic operation, a pseudo-inductive behaviour is observed in the low frequencies region (< 3 Hz).[97-99] And, under potentiostatic control this behaviour is observed at a critical potential, which is coincident with the ignition potential and is dependant on the catalyst in use.[100]

The segmented spatial electrochemical impedance spectroscopy (EIS) studies presented by Reshetenko *et al.* (2012 and 2014) evaluated the dynamic response of a cell exposed to 2 ppm CO/H_2 in H_2/O_2, H_2/air and H_2/H_2 systems. In previous studies, it was assumed that under galvanstatic control the changes in the EIS spectra were due exclusively to anode contributions.[97, 99] In this study, it was found that there is an increase of charge transfer resistance for both, the anode and the cathode, confirming that the CO also impacts the electrochemical processes in the cathode. Additionally, the pseudo-inductive behaviour at low frequency was observed in the first segments of the cell (more severely contaminated) for H_2/air and H_2/H_2 systems, which was attributed to the surface relaxation of the anode, related to the competitive electrochemical oxidation of H_2 and CO. The electric equivalent circuit was adapted to include this contribution. For this concentration, the H_2/O_2 operation did not present this behaviour due to the predominance of the direct chemical oxidation of CO by the diffused O_2.[82, 83]

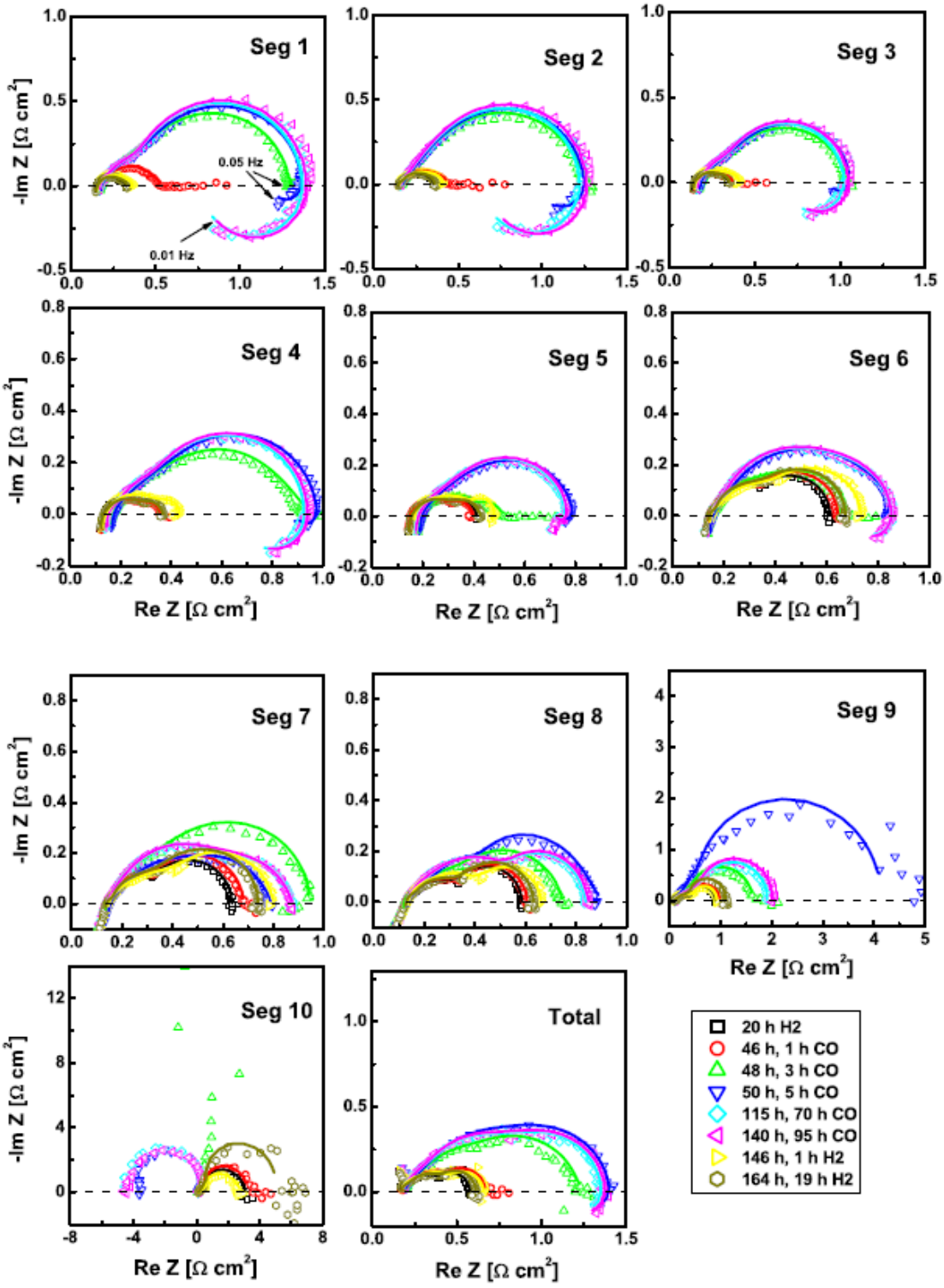

Figure 15. Electrochemical impedance spectra evolution obtained for a segmented cell exposed to 2 ppm CO. The ten segments follow a serpentine flow, where segment 1 is closer to the anode inlet. A pseudo-inductive behaviour is observed in the first segments in a H_2/air system. The experimental data is represented by symbols, while the modelling results by solid lines. Reproduced with permission.[83] Copyright 2014, Elsevier.

3. Mitigation strategies

The development and optimization of mitigation strategies that could enhance the CO tolerance of fuel cells is a major area of interest. Various mitigation strategies have been proposed in order to reduce the CO content after the first stage of purification is achieved by the WGS reaction. The CO concentration after this process reaches up to 3%.[14] According to the means by which the technologies are applied, these can be divided into three groups: (i) the pre-treatment of reformate; (ii) 'on board' CO removal, and (iii) in-operando strategies (Figure 16). Their development follows different approaches that include the development of new materials, the supply of feed gases, variation on the operating conditions, or the modification of the MEA. An overview of the proposed techniques is presented in this section. The choice of the technique will depend on the specific requirements of the system.

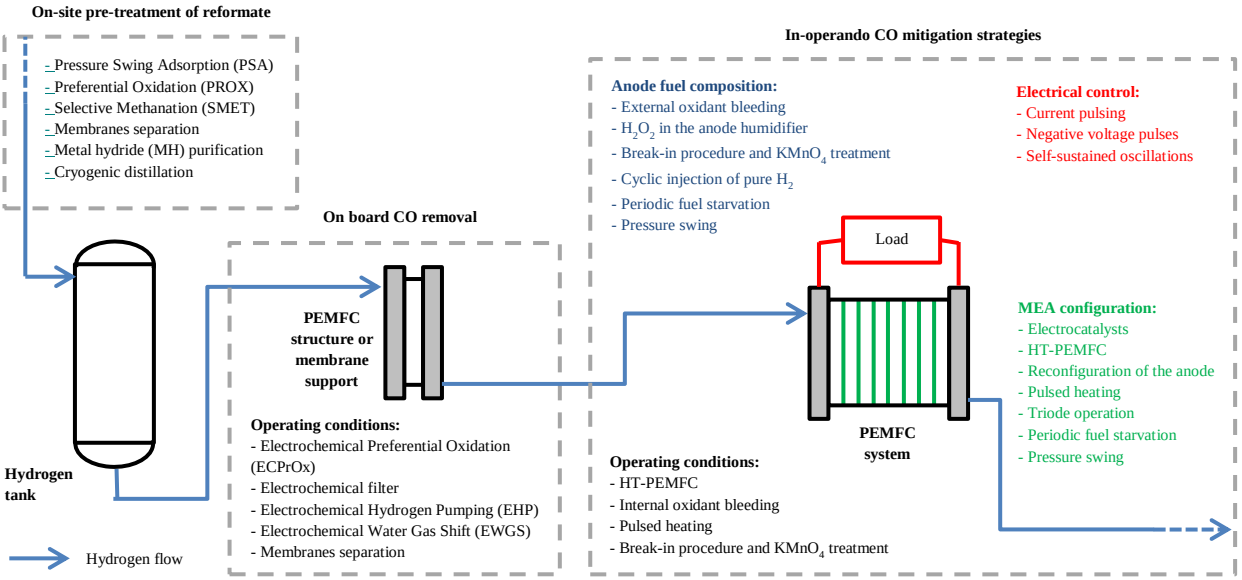

Figure 16. Summary of the proposed mitigation strategies for CO poisoning in PEMFCs.

3.1 Pre-treatment of reformate

The processes described here are well-established on-site technologies. Although there are more options available for the separation of hydrogen, here the focus is on the removal of CO and summarised in Table 1. The maximum concentration of CO obtained after these processes is 10 ppm CO. There are different categories, including adsorption, membranes, scrubbers, and selective reaction. Around 85% of the hydrogen production units worldwide use the pressure swing adsorption (PSA) as the purification process.[13]

Table 1. Most deployed pre-treatment technologies for the removal of CO from reformate

Mitigation strategy	Subdivision	Advantages of the technique	Disadvantages of the technique	Scale of use	Hydrogen output (%)		Comments	References
					Purity	Recovery		
Pressure Swing Adsorption (PSA)	N.A.	- Fast and continuous without the disruption of the regeneration processes of the adsorbents. - The produced H_2 is at the same pressure as the feed.	- In order to reach high removal efficiencies, a high pressure (between 5 and 10 bar) is needed. - The process requires complex operation.	Large	99-99.999%	70-85%	- 85% of the hydrogen produced worldwide is purified through this technique.	101-104
Preferential Oxidation (PROX)	N.A.	- Small amounts of CO react in the presence of large quantities of H_2. - Continuous operation. - Low energy is necessary for the provision of oxygen as it comes from air.	- Careful control of the O_2/CO ratio is needed. - The risk of a spontaneous explosion. - Bulky and complex system. - The hydrogen is consumed as a side reaction.	Small	99.999%			13, 15, 105, 106
Selective Methanation (SMET)	N.A.	- No other gas is needed for the reaction to take place. - No advanced controls needed.	- High hydrogen waste. - Low performance of the Ni- and Ru- based catalysts used.	Small	99.999%			15, 105, 106
Selective Membranes	Pd based membranes	- Separation in one step. - Low energy consumption. - Continuous operation. - Mild conditions of separation. - High selectivity of H_2. - Capability of scaling.	- Fouling tendency. - Low membrane lifetime. - High costs. - Other contaminants, such as N_2.and CH_4, are not removed.	Small to large	99.9999%	< 99%	- Other types of membrane are available. However, the dense metallic membranes, especially the Pd alloys are more suitable for hydrogen separation.	13, 102-104, 107, 108
	Two-dimensional membranes	- High selectivity. - High permeability. - Removal of different contaminants, sucha as CH_4 and CO_2.	- Limited or inexistent experimental preparation of the materials. - Lack of experimental studies about the purification of H_2.				- In the case of graphene, controlling the pores size and the homogeneous distribution is a challenge.	109, 110
Metal Hydride Separation	AB_5- type alloys	- Simple device. - Low energy consumption. - Simple and safe operation. - High recovery ratio of hydrogen. - Hydrogen is stored at the same time.	- The H_2 alloys used so far for purification have low storage capacity. - Deterioration of the performance in the presence of impurities such as O_2, H_2O, CO, sulphur containing species, etc. - Limited capacity for the purification of CO.	Small to medium	< 99.9999%	75-95%	- The composition of the feed gas has a great impact on the rate of absorption and hydrogen purity obtained.	102, 104, 108, 111
Cryogenic Distillation	N.A.	- Possibility to store hydrogen as a liquid.	- High costs. - Energy-intensive. - High consumption of liquid nitrogen.	Large	90-99%	95%	- The purity obtained depends on the operating temperature, pressure and the composition of the stream.	12, 102, 103

3.1.1 Pressure Swing Adsorption (PSA)

PSA is a non-cryogenic gas separation process that uses adsorbent technology to obtain hydrogen with a purity between 99% and 99.999%.[102-104] The reformate is placed in a packed column at high pressure, where the impurities are selectively adsorbed by highly porous materials. Multiple adsorbents, such as zeolites, activated carbons, and silica and alumina gels are placed in individual layers inside the column. The retention of impurities depends on the affinity between the adsorbent and the gas molecule.[8, 13] Once the impurities have been adsorbed, the pressure is lowered to regenerate and purge the column. Typically, at least three cyclic columns are operated simultaneously.[8]

PSA presents several advantages. It is fast and allows the continuous purification of hydrogen without disrupting the regeneration process of the adsorbents, which are used several times before losing their adsorptive capacity. Additionally, the hydrogen produced is at the same pressure as the feed.[112] The drawbacks are the need for high pressure (between 5 and 10 atm) in order to achieve high removal efficiencies, and the process generally requires a complex operation under a series of sequential, non-isothermal, non-isobaric and non-steady-state process steps. The main areas of research for this process are the hydrogen recovery at high purity, the decrease in the amount of adsorbent needed and the hardware costs.[13]

3.1.2 Preferential Oxidation (PROX)

In this process, air is supplied to the reformate gas in the presence of a catalyst. The main reaction is:[15]

$$\mathbf{2CO + O_2 \rightarrow 2CO_2} \qquad \mathbf{\Delta_r H^{\circ}_{298} = -566\ kJ/mol} \qquad \mathbf{(9)}$$

An undesirable side-reaction is:

$$\mathbf{2H_2 + O_2 \rightarrow 2H_2O\ (gas)} \qquad \mathbf{\Delta_r H^{\circ}_{298} = -484\ kJ/mol} \qquad \mathbf{(10)}$$

The process reduces the CO content to 50-100 ppm.[105] The main advantage of this process is that a small amount of CO reacts in the presence of large quantities of H_2. The process can operate on a continuous basis. Additionally, as the oxygen necessary for the reaction comes from air, low energy is required for its provision and the process can operate at atmospheric pressure.[13] However, this process presents several challenges: the need to control the concentration ratio O_2/CO and the risk of spontaneous explosion due to the gas mixture. The system is bulky and complex as a consequence.[15] Another problem is the consumption of hydrogen by the reaction (9).[105]

The catalysts developed are mainly supported Ru and Pt-based alloy catalysts. The advances have been focused on the development of catalysts able to operate over a broader range of temperature, as well as at low temperature to avoid the reverse water-gas shift reaction.[106] Park *et al.* (2009) presented a comprehensive review of the different advances made on this technology.[106]

3.1.3 Selective Methanation (SMET)

The target reaction for the selective methanation (SMET) is:[15]

$$\mathbf{CO + 3H_2 \rightarrow CH_4 + H_2O} \qquad \mathbf{\Delta_r H^{\circ}_{298} = -206\ kJ/mol} \tag{11}$$

The side-reactions are CO_2 methanation and reverse WGS:

$$\mathbf{CO_2 + 4H_2 \rightarrow CH_4 + 2H_2O} \qquad \mathbf{\Delta_r H^{\circ}_{298} = -165\ kJ/mol} \tag{12}$$

$$\mathbf{CO_2 + H_2 \rightarrow CO + H_2O} \qquad \mathbf{\Delta_r H^{\circ}_{298} = +41\ kJ/mol} \tag{13}$$

SMET is a promising technology as there is no need for another gas for the reaction to take place.[106] Additionally, the process is free of nitrogen dilution, avoiding the danger of explosion and the need for advanced controls that PROX requires. The primary challenge that this process presents is the low performance of the Ni- and Ru- based catalysts.[15] Park presented a comparison of the catalytic performance for the SMET, and emphasised the focus of the research on increasing the catalyst selectivity to remove CO in the presence of an excess of CO_2 and H_2.[106] Another challenge to overcome is the high hydrogen waste.[15]

3.1.4 Membranes separation

3.1.4.1 Pd-based membranes

Over the past 50 years, membrane separation has received much attention for different applications, including micro-filtration of bacteria to reverse osmosis for water clean-up.[103, 113] There are several membranes for hydrogen separation. Considering the material they are made of, they can be divided into different categories: polymer, metallic, carbon and ceramic.[103, 107, 114] Another classification would be between porous and dense. For the hydrogen separation, porous membranes use the molecular sieving as a primary mechanism, while the dense membranes utilise solution diffusion.[103]

Palladium and its alloys have been the most studied membranes for hydrogen separation, due to palladium's high catalytic activity for hydrogen dissociation and its high permeability for diffusion of hydrogen atoms.[106, 107] Considering that palladium membranes are susceptible to embrittlement below 300 °C, and their tendency to suffer sulphur and carbon monoxide poisoning at low temperatures, Pd-based alloy membranes have been developed to overcome these effects and to enhance the hydrogen permeability. Figure 17 presents the processes involved using this class of membrane[103] which can achieve a purity of up to 99.9999% H_2.[102]

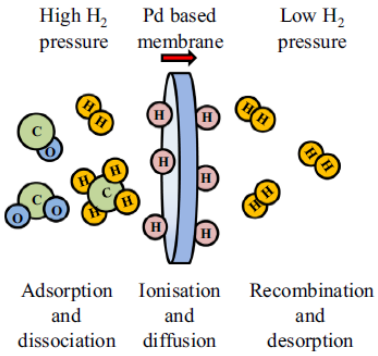

Figure 17. Processes involved in the separation of hydrogen from a hot gas mixture through a Pd-based membrane. Reproduced with permission.[103] Copyright 2015, Elsevier.

However, not all the Pd-alloy membranes are resistant to the presence of certain species, in particular, H_2S hinders the permeability of hydrogen.[107, 114] The costs are another disadvantage of Pd-based membranes. Thin metallic membranes have been developed to reduce costs and increase the hydrogen flux.[114] Due to the reduced thickness, membranes are deposited onto substrates to provide mechanical support. Different materials have been proposed, from which porous stainless steel (PSS) has proved to provide strength, robustness, similar thermal expansion and ease of welding and sealing.[103] Most Pd-based membrane research is focused on optimizing the alloys and creating new fabrication methods.[107]

3.1.4.2 Two-dimensional membranes

Two-dimensional materials have emerged in the development of membranes due to their high selectivity and permeability. Highly specific separations are achieved under high flux rates.[109] In the case of graphene-based membranes, produced from graphene, graphene oxide and chemically converted graphene materials, three main types of membranes exist according to their microstructure (Figure **18**): porous graphene layer, assembled graphene laminates and graphene-based composite.[115] The three types of membranes have been considered for the purification of H_2[115], although for the H_2/CO separation the theoretical studies of porous membranes stand out. A few examples are the two-dimensional polyphenylene,[116] the PG-ES1[117] and the nitrogen-substituted porous graphene monolayers 3N-PG and 6N-PG.[118]

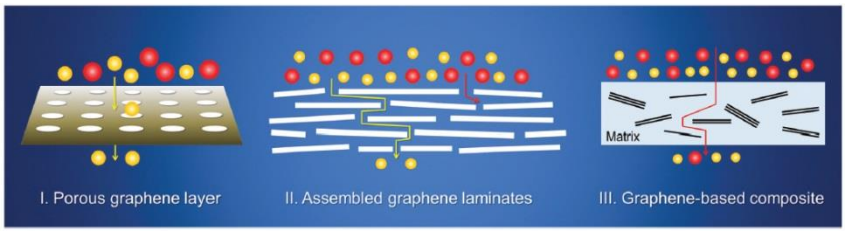

Figure 18. Diagram of the microstructures of the main types of graphene-based membranes: porous graphene layer (type I), assembled graphene laminates (type II) and graphene-based composite (type III). Reproduced with permission.[115] Copyright 2015, The Royal Society of Chemistry.

Controlling graphene with specific pore sizes and homogeneous distribution is a challenge, hence the interest in other two-dimensional carbon allotropes with uniformly distributed pores.[110] Among them is graphdiyne,[119] whose framework is formed by hexagonal carbon ribs linked by diacetylene.[120] For the separation of CO/H_2, several theoretical studies have evaluated the properties of the elemental graphdiyne,[121, 122] while others have modified the structure to enhance the purification capabilities in the cases of nitrogen modified graphdiyne[123] and charge-modulated graphdiyne.[124] Other two-dimensional membranes under study for the CO/H_2 separation include the rhombic graphyne,[125] the g-C_3N_3[110] and C_3N_4[126] monolayers, the strain-controlled nanoporous graphenylene[127] and the inorganic graphenylene,[128] among others. While the predicted properties of these materials are promising for the purification of H_2, their preparation and characterisation is limited. An advantage these membranes would present (depending on the material) compared to other mitigation strategies would be the removal of other species such as CO_2 and CH_4, also present in the reformate.[109]

3.1.5 Metal hydride (MH) purification

Metal hydrides (MH) are one of the most promising materials for the storage of hydrogen due to their applicability in stationary, mobile and portable applications, their efficiency and safe use.[129] Since the 1970s, the use of metal hydrides has been extended for hydrogen separation and purification.[111] The mechanism is based on the selective adsorption of molecular hydrogen on the metal or alloy surface under certain conditions of temperature and pressure. The hydrogen is decomposed into atoms, forming a solid solution MH_x, followed by formation of the metal hydride MH_y. The hydrogen is stored, which constitutes one of the main advantages of the system. When desorbed, the impurity gases are purged first.[108] The most deployed MH for separation and purification of hydrogen are the AB5-type.[111]

Among the advantages that these devices present are their simplicity, low energy consumption, relatively safe use and straightforward operation, as well as the high purity reached (up to 99.999%).[108] Major challenges include the impact of the composition of the fed gas on the final composition, the rate of absorption and the long-term stability. The most severe contaminants are CO, O_2, H_2O and sulphur-containing compounds.[108, 111] Hence, MHs have a serious limitation regarding removal of CO. However, Modibane *et al*. (2013) reported substrates $La(Ni, Co, Mn, Al)_5$ with stable performances over gas mixtures containing 10% CO_2 and 100 ppm CO.[111] Concurrently, Miura *et al*. (2012) proposed a system for start and stop operations, composed by several units connected in series. In the first one, the CO is removed by an adsorbent, while the hydrogen was stored in the following units. The process is called CO adsorption metal hydride intermediate buffer (COA-MIB), and 83% of hydrogen recovery was achieved after one month of operation. Figure 19 presents the operation of the COA-MIB,[130, 131] and common AB5-type alloys.[111]

(a) **(b)**

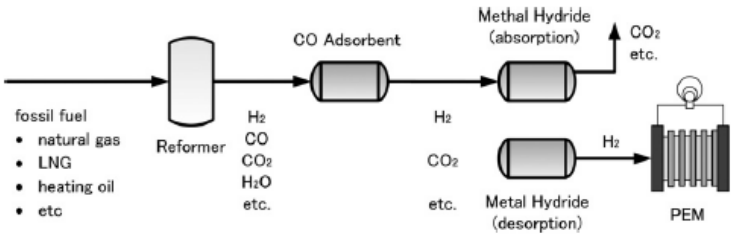

Alloy	Absolute [H/AB$_5$]		Reversible	
	Absorption (80 °C / 2.5 bar)	Desorption (200 °C / 1 bar)	[H/AB$_5$]	[cm^3/g STP]
LaNi$_4$Mn	5.205	1.252	3.953	104
LaNi$_4$Mn$_{0.5}$Co$_{0.3}$Cu$_{0.2}$	3.306	0.092	3.214	85
La$_{0.34}$Ce$_{0.50}$(Pr,Nd)$_{0.16}$ Ni$_{3.15}$Co$_{0.65}$Mn$_{0.6}$Al$_{0.6}$	3.937	0.192	3.745	99
LaNi$_{3.55}$Co$_{0.75}$Mn$_{0.3}$Al$_{0.4}$	5.035	0.368	4.667	124

Figure 19. Metal hydride reactor for hydrogen separation and purification. (a) operation of the CO-MIB system. Reproduced with permission.[130] Copyright 2012, Elsevier. (b) Hydrogen sorption capacities of common AB$_5$- type alloys. Reproduced with permission.[111] Copyright 2013, Elsevier.

3.1.6 Cryogenic distillation

The cryogenic distillation or partial condensation is based on the difference in volatility of the components on the gas stream.[12, 132] The process is performed at low temperatures at which the impurities condense, while the hydrogen remains in the gaseous phase due to its low boiling point (-252.9 °C). The efficiency of the process depends on the operating temperature and pressure, and the composition of the feed.[104] This process has been used for the separation of the different hydrogen isotopes.[12] The separation is highly energy intensive and costly. An additional disadvantage is the limited purity that is reached compared to other processes, which typically reaches ~99%.[103]

3.2 On-board removal of CO

In recent years, some on-board hydrogen purification technologies have emerged. Their structure is similar to PEMFCs; however, their operation is focused on the purification of the stream, and not the generation of energy. An external power supply is required, and they are placed in-line before the fuel cell stack. A common advantage is the generation of power, or in particular cases, the consumption of almost null power. Although promising results have been obtained, the optimization of these technologies is vital to be able to compete with the conventional in-site purification processes. A summary of these technologies is presented in Table 2.

Table 2. On-board removal of CO from hydrogen for its use in PEMFCs.

Mitigation strategy	Subdivision	Stream with the highest reported CO content in the anode	Advantages of the technique	Disadvantages of the technique	Comments	References
Electrochemical Preferential Oxidation (ECPrOx)	N.A.	H_2/24.1% CO_2/9380 ppm CO	- CO is removed without any H_2 or CO waste. - The operation is feasible at room temperature, high anode pressure, atmospheric air pressure, and without external humidification. - Supplemental electrical power is produced. - The use of electrical power as an additional tool to enhance the oxidation of CO. - It is possible to cascade several ECPrOx reactors, depending on the initial CO concentration in the reformate.	- A heat exchanger might be needed in order to reach the optimal operating conditions. - Relatively new, it has not been tested in the industry.		105
Electrochemical Filter	N.A.	10,000 ppm CO/H_2	- The size of the filter is scalable according to the concentration of CO.	- The volume of the filter increases as the concentration of CO. To reduce 10,000 ppm to 10 ppm the volume of the filter occupies up to 10 times the one of the cell.	- The combined use of a PrOx reaction and an electrochemical filter can be used to reduce the volume of the filter, over high concentrations of CO.	16, 18, 133
Electrochemical Hydrogen Pumping (EHP)	High Temperature (PBI membranes)	74.7% H_2, 1.36% CO, 23.5% CO_2 and 0.36% CH_4	- Removal of other contaminants, such as CO_2 and N_2. - Simultaneous separation and compression of hydrogen. - The power requirements are minimal. - Excellent stability and durability. - Fast dynamic response.	- An increase in the inlet pressure enhances the hydrogen generation, but decreases the purity of it.	- The generation of hydrogen is dependent on the applied current.	134-136
	High-temperature EWGS	50 mol% H_2, 50 mol% CO	- Simultaneous generation and separation of H_2 - Mitigation of high concentrations of CO.	- Limited studies about the mechanisms involved.	- The reported concentration is prior to humidification.	137, 138
	Periodic current pulsing	80% H_2 with 1000 ppm CO / 20% CO_2	- Low temperature operation. - Removal of other contaminants, such as CO_2 and N_2. - Simultaneous separation and compression of hydrogen.	- Under short-circuit conditions, the anode potential might reach values above the thermodynamic stability limit, decreasing its catalytic activity.	- So far little research and optimisation of the system have been made.	139
	EWGS at ambient temperature	100 ppm CO/H_2	- High efficiency, as CO is used to generate H_2. - Low energy consumption. - Removal of other contaminants such as NO, H_2S, CS and CO_2. - Safe to use.	- Limited studies of the mechanisms.	- The use of a liquid electrolyte is proposed in order to increase the CO adsorption.	140

Table 3. On-board removal of CO from hydrogen for its use in PEMFCs.

Mitigation strategy	Subdivision	Stream with the highest reported CO content in the anode	Advantages of the technique	Disadvantages of the technique	Comments	References
Hydrogen purification membranes	Al_2O_3-supported Si_3N_4 membrane	1% CO/H_2	- Continuous separation of CO. - Low energy consumption. - High tolerance. - Low cost and ease of fabrication of Si_3N_4. - Capability of scaling.	- Limited understanding of the separation mechanisms. - The need of a converter for the disposal of CO.		141

3.2.1 Electrochemical Preferential Oxidation (ECPrOx)

Electrochemical preferential oxidation (ECPrOx) has been proposed as an alternative to conventional PrOx.[105] The structure of the ECPrOx units is similar to that of the PEMFC. The difference is the operation, which is based on the spontaneous potential oscillations the cells exhibit due to the exposure to CO under galvanostatic control (Section 2.2.2). The objective is to enhance the adsorption of CO and its oxidation to CO_2, so the concentration of CO in the stream is reduced before entering the fuel cell. Figure 20 shows how the system integrates the ECPrOx and PEMFC.[105]

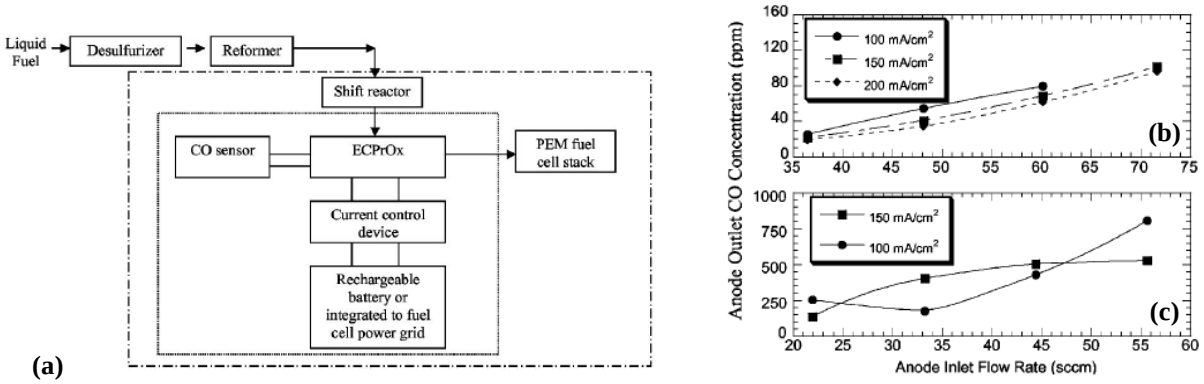

Figure 20. (a) Integration of the ECPrOx unit into a reformer-fuel cell system, (b) and (c) anode outlet concentration of CO as a function of inlet flow rates at different current densities over the exposure to 1000 ppm CO/H_2 and 9380 ppm CO/24% CO_2 /75% H_2 respectively. Reproduced with permission.[105] Copyright 2005, The Electrochemical Society, Inc.

The advantages of the ECPrOx compared to PrOx are the CO removal without H_2 waste and the supplemental electrical power produced. The ECPrOx can take place at room temperature, atmospheric air pressure, and with no external humidification. A high anode pressure facilitates the CO adsorption, lowering the concentration of CO at the anode outlet. Moreover, the use of electrical potential is used to enhance the electro-oxidation of CO. As the efficiency is increased at lower temperatures, a heat exchanger might be needed prior to the ECPrOx unit.[105]

Hanke-Rauschenbach (2009) studied the oscillatory behaviour of potential using the model presented by Zhang et Datta (2002) as a base, and compared the behaviour of two ECPrOx reactors with electrical connections in series and in parallel.[42, 142] It was concluded that the CO conversion is improved in the series system due to the independent oscillations of each unit. The units connected in parallel oscillate simultaneously, affecting the performance of the system.[142] This comparison is supported by the experimental results obtained by Lu *et al.* (2009),[143] and also by Heidebrecht *et al*. (2012), who presented a design approach for cascades of ECPrOx, using a degrees-of-freedom analysis.[144]

3.2.2 Electrochemical filter

Lakshmanan *et al.* (2002) were the first to show how a PEMFC operating under pulse potential control could be used as a filter to remove CO from reformate.[16] In order to ensure constant operation, the system involves the use of two PEM fuel cells that alternately cycle between CO adsorption and CO oxidation.[133] Figure 21 shows how reformate enters the anode of the first cell (F1), which is operated at open-circuit. The CO is adsorbed on the catalyst surface, effectively filtering

the CO from the stream, the remaining 'purified' hydrogen-rich gas entering the second fuel cell. After a switching time, when most of the catalyst surface is covered by CO, the reformate enters into the second cell (F2 in the diagram). A potential pulse is then applied to F1 that allows the oxidation of CO.[18, 133, 145]

A fixed-bed adsorber model was used to optimise the switching time and different operating conditions. It was possible to reduce the concentration of CO from 10,000 ppm to 10 ppm at 25 °C, using a flow 100 cm^3 min^{-1}, a catalyst charge of 4 mg Pt cm^{-2} and a switching time of 20 s. The potential for the CO oxidation was 0.7 V. A primary consideration to take into account is the volume of the 'filter' to remove high concentrations of CO. For instance, reducing the concentration of CO from 10,000 ppm to 10 ppm to feed a cell operating at 1 A cm^{-2}, requires a filter cell almost ten times the area of the fuel cell.[18]

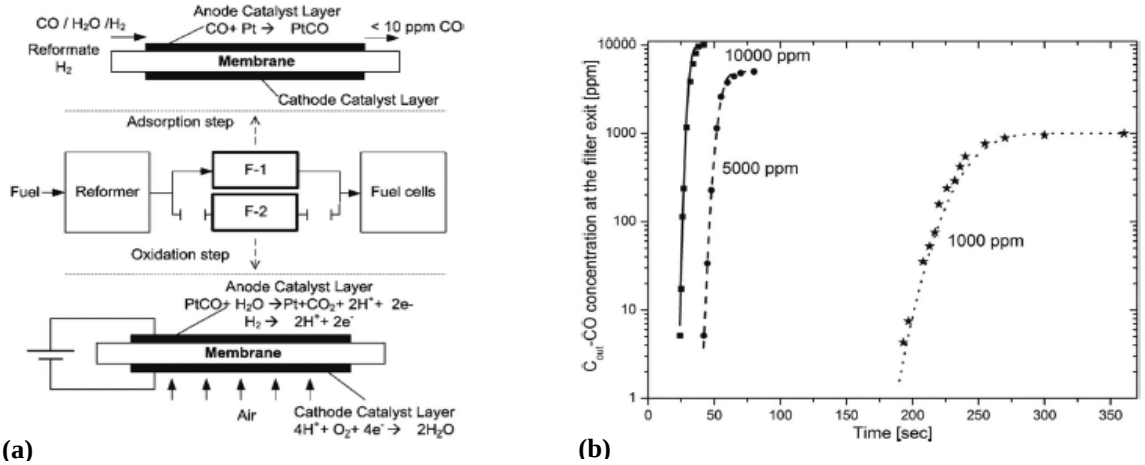

Figure 21. Electrochemical filter: a) diagram showing the two PEMFCs operating over the adsorption and oxidation steps, b) experimental (symbols) and model fit (lines) for different CO/H_2 concentrations at 25 °C, 100 cm^3 min^{-1} and 4 mg Pt cm^{-2}. Reproduced with permission.[18] Copyright 2015, The Electrochemical Society, Inc.

3.2.3 Electrochemical hydrogen pumping (EHP)

Electrochemical hydrogen pumping is a technology originally presented in the 1960s, with the main objective of purifying and compressing hydrogen.[146, 147] As shown in Figure 22, the mixed stream enters the anode, where the hydrogen is oxidized. The protons 'pumped' to the cathode where pure and pressurized hydrogen is collected.[148]

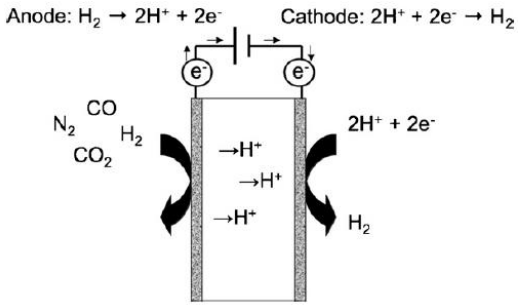

Figure 22. Diagram illustrating the operation of an electrochemical hydrogen pump, separating hydrogen from a mixture of gases in the anode. Reproduced with permission.[134] Copyright 2008, Elsevier.

The EHP can separate the hydrogen as long as the components of the stream do not poison the catalyst, so that the technology was not considered for the separation of CO.[149] The introduction of EHP at high temperature PEMFC with phosphoric acid-doped PBI membranes (Section 3.3.2),[134] and EHP combined with other techniques such as the current pulsing operation (Section 3.3.9)[139] and the enhancement of the Electrochemical Water Gas Shift (EWGS)[137, 138] offered the possibility of CO mitigation at high levels.

3.2.3.1 High-temperature EHP

Studies have reported the separation of CO through EHP at high temperatures using phosphoric acid-doped PBI membranes. Perry *et al.* (2008) evaluated a non-humidified stream containing 35.8% H_2, 11.9% CO_2, 1906 ppm CO and N_2 balance at 160 °C. At 0.4 A cm^{-2}, the outlet stream had a concentration of 11 ± 1 ppm CO and 0.37 ± 0.09 % CO_2. Higher hydrogen purity was obtained by increasing the current to 0.8 A cm^{-2}, obtaining 13 ± 3 ppm CO and 0.19 ± 0.02 % CO_2. It was also demonstrated that the long-term durability could reach up to 4000 hrs.[134] Thomassen *et al.* (2010) evaluated a different range of temperatures for the separation of CO (Figure 23), and demonstrated the fast dynamic response and the stability of the system.[135]

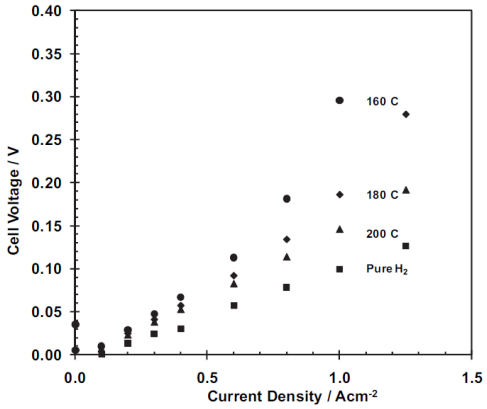

Figure 23. Polarisation curves at different temperatures of a PBI-based EHP unit, fed with a reformate mixture containing 74.7% H_2, 1.36% CO, 23.5% CO_2 and 0.36% CH_4. Reproduced with permission.[135] Copyright 2010, Elsevier.

3.2.3.2 Electrochemical water gas shift (EWGS)

The Electrochemical Water Gas Shift (EWGS) combines the separation of H_2 through the EHP, and the electrochemical CO oxidation. In the case of the EWGS at high temperatures (between 130 and 150 °C), PBI membranes were used as the electrolyte. Both the EHP and the electrochemical CO oxidation occur simultaneously at high current densities, and with a feed containing high concentrations of CO and H_2O. A diagram of the processes involved, and a typical polarization curve, are presented in Figure 24. Oettel *et al.* (2012) tested concentrations up to 50 mol% H_2 and 50 mol% CO (prior to humidification) achieving exergy efficiencies as high as 43.3%.[137, 138]

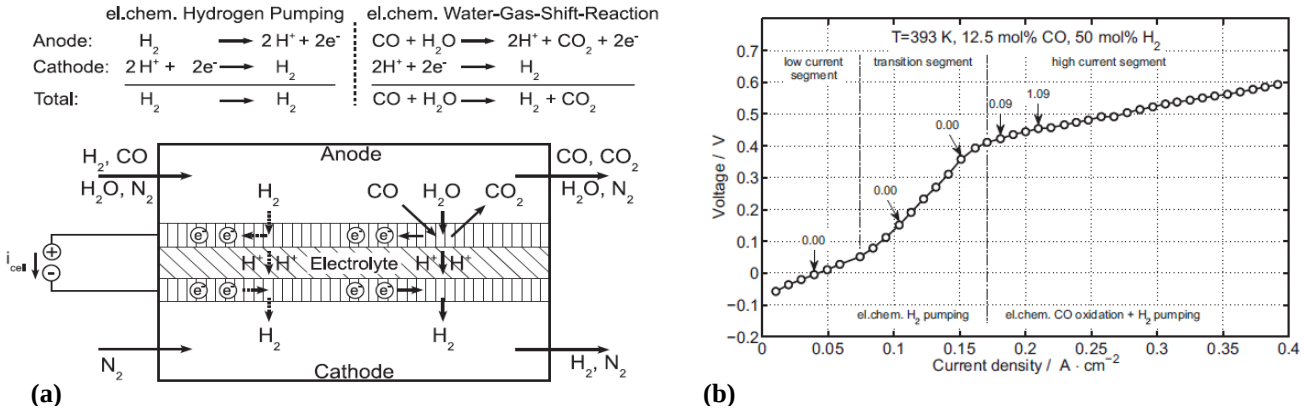

Figure 24. Electrochemical water gas shift reactor (EWGSR): (a) diagram showing the simultaneous generation and separation of hydrogen; (b) typical polarization curve obtained at 393 K, showing the operation of the EHP (transition current segment) and the EWGS (high current segment). The anode feed contained 12.5 mol % CO and 50 mol% CO (subsequently humidified). The concentration of CO_2 in the anode outlet was determined for five points, through GC analysis. Reproduced with permission.[137] Copyright 2012, Elsevier.

3.2.3.3 Current pulsing in EHP

At room temperature and atmospheric pressure, Gardner *et al*. (2007) tested the application of anodic current pulses in an EHP unit, for the separation of CO from a stream containing a mixture of 80% H_2 with 1000 ppm CO/20% CO_2. The cell pulsing substantially reduced the separation efficiency, even though the performance of the unit is better with no CO (Figure 25). A model representing the separation of hydrogen was also presented, taking the model from Zhang (2004) as a basis.[139, 150]

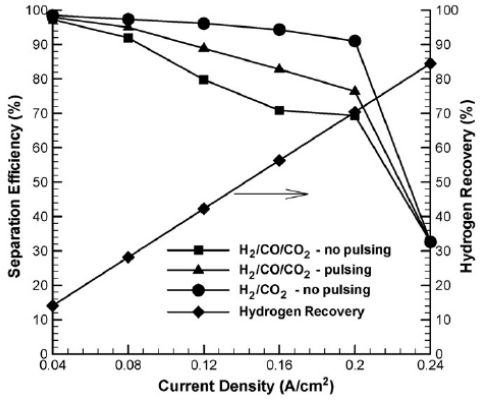

Figure 25. Effect of the current pulsing technique in the anode of a EHP unit over the exposure to different compositions of gases: ● no pulsing, 80% H_2 and 20% CO_2; ▲ pulsing, 80% H_2 with 1000 ppm CO/20% CO_2; ■ no pulsing, 80% H_2 with 1000 ppm CO/20% CO_2; ♦ hydrogen recovery. Reproduced with permission.[139] Copyright 2007, Elsevier.

3.2.3.4 EWGS at ambient temperature

A study on the separation of H_2 in combination with the electro-oxidation of CO was presented by Huang *et al*. (2006). The EHP operation was done at ambient temperature, until the complete coverage of the catalyst by CO. The operation was then interrupted, and a fraction of the power generated by the subsequent fuel cell was applied into the reactor to operate as an electrolyser. The OH^- molecules generated in the anode contributed to the electro-oxidation of CO. The system response showed that it could mitigate a stream containing 100 ppm CO/H_2. The process has the advantage of using the CO as a reducing reagent to produce additional H_2 from water. Other advantages are the removal of other contaminants, that include hydrogen sulphide (H_2S), carbonyl monosulfide (CS), carbon dioxide (CO_2), and nitrogen oxide (NO); and inherently safe use compared to other technologies.[140] A diagram showing the processes involved is presented in Figure 26, as well as the evolution of the voltage over its operation. Additionally, the use of a liquid electrolyte in order to increase the CO adsorption capacity of the reactor was reported.[140]

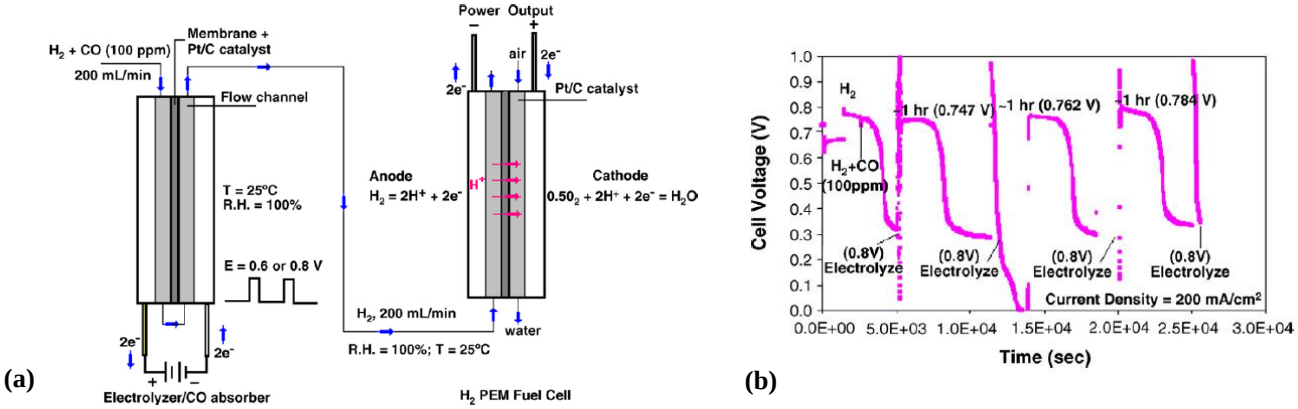

Figure 26. Electrochemical water gas shift (EWGS): (a) Diagram of the process, (b) performance of the fuel cell fed with the stream coming from the EWGS unit. The fuel entering the unit contained 100 ppm CO/H_2. Reproduced with permission.[140] Copyright 2006, Elsevier.

3.2.4 Membranes separation

In recent years, the use of membranes has broadened to the on-board purification of hydrogen. Liu *et al.* (2013) presented an Al_2O_3-supported Si_3N_4 membrane capable of removing CO from a stream containing 1%CO/H_2. The separation occurred through a combination of chemisorption and physisorption processes, and the resultant hydrogen fed the fuel cell operating on-line. The CO was disposed through a bypass needle valve. With the membrane in place and in the presence of CO, the decrease in power density was less than 0.01 W cm^{-2}. An advantage of this technique is the low cost and ease of fabrication of Si_3N_4, although more research is needed for the understanding of the mechanisms in place, and to determine the efficiency of the membrane in the case of long exposures to CO.[141] Another consideration is the need of a converter for CO, as in this study it is directed to the exhaust.

3.3 In-operando mitigation strategies

Several *in operando* techniques have been developed to mitigate CO poisoning in PEMFCs; these follow a range of approaches including the development of new materials, the variation of the conditions of operation, the change of fuel cell design and/or the addition of new components. In general, the objectives are to allow operation of cells at a high concentration of CO (up to that delivered at the exit of a reformer), be of simple design and economically feasible. Of these approaches, the development of CO tolerant catalysts is the most examined, followed by air-bleeding and high-temperature operation. Table 4 presents the advantages and disadvantages of each approach.

Table 4. In-operando mitigation strategies for CO poisoning in PEMFC

Mitigation strategy	Subdivision	Stream with the highest reported CO content in the anode	Advantages	Disadvantages	Comments	References
Electrocatalysts	Platinum-based catalysts	2000 ppm CO/H_2	- Different structures and compositions are available. - No alteration of the configuration of the cell.	- Scarcity and high costs of platinum - The stability of Pt alloys in the long term is limited.	- Pt-Ru catalysts are the most effective against CO poisoning in the market and the most durable, although they are less stable than Pt.	19, 151-157
	Non-platinum catalysts	1% CO/H_2	- Different structures and compositions are available. - Lower costs compared to Pt-based catalysts	- Low activity for HOR in most cases. - Limited studies about the durability of the catalysts.	- The tests performed in the presence of 1%H_2/CO were done in half-cell tests. This concentration has not been tested in real fuel cell conditions.	158-160
High-temperature fuel cells	N.A.	5% CO/H_2	-The use of direct reformate is possible, simplifying the balance-of-plant. - Simplification of water management and heat rejection. - The contamination by H_2S can also be mitigated.	- Most membranes are susceptible to dehydration at high temperature, resulting in low conductivity. - The phosphoric acid blocks the surface of the Pt, limiting the ORR in the cathode. - Fast-start capabilities are limited compared to conventional PEMFC. - A corrosion mechanism can be activated due to the elevated temperatures.	Jiao *et al*. (2013) presented numerical simulations with various flow channel designs, considering a CO concentration to up to 20%.	161-168
Oxidant bleeding	External bleeding	10,000 ppm CO/H_2	- High efficiency against CO poisoning. - Limited concentrations of H_2S can also be mitigated	- Fuel utilization rate is diminished. - Increased temperature reduces the anode lifetime due to sintering of the catalyst. - Can promote the formation of pin-holes in the membrane after extended operation due to the formation of H_2O_2. - Careful control is needed over air supply. - High concentrations of CO are not mitigated in the long run. - Fuel efficiency limited due to the production of water in the anode	- Oxygen bleeding is less effective for lower CO concentration, lower catalyst loading and thin electrodes.	169-172
	H_2O_2 in the anode humidifier	100 ppm CO/H_2	- High efficiency. - Safer than the external bleeding.	- The concentration of CO that can be mitigated is limited. - The presence of H_2O_2 provokes degradation of the membrane in the long-term.		66, 153, 171, 173

Table 5. In-operando mitigation strategies for CO poisoning in PEMFC (continuation)

Mitigation strategy	Subdivision	Stream with the highest reported CO content in the anode	Advantages	Disadvantages	Comments	References
Oxidant bleeding	Internal bleeding	0.24% CO/12.82% CO_2/ 12.84% H_2/12.18% N_2/ 61.92% He	- Simple application. - Effective in mitigating CO poisoning.	- Reduced thickness of the membrane enhances CO crossover to the cathode and the decrease of the membrane conductivity. - Crossover of oxygen can produce H_2O_2, which can degrade the membrane.		34, 149, 171, 174
Reconfiguration of the anode	Bilayer anode structure	5000 ppm CO/H_2	- In most cases the amount of catalyst is reduced without affecting the performance. - Lifetime of the cells is extended if it is combined with oxidant bleeding. - Can also be used to mitigate CO_2 contamination.	- Careful control for the oxidant bleed is required. - High consumption of platinum in the case of the PtMo/PtRu bilayer.	- The method of preparation of the layers has an important influence on the concentration of CO that can be tolerated.	152, 175-180
	Refined diffusion layer	100 ppm CO/H_2	- The heating effects of the oxidant bleeding are not observed, and the lifetime of the cell is extended if combined with oxidant bleeding.	- Careful control for the oxidant bleed is required. - Limited studies about the distribution of the particles in the GDL.	- The catalytic activity of Au particles depends mostly by the size and the distribution of the particles, even though its high activity for WGS reaction.	181, 182
	Complementary composite film coating	100 ppm CO/H_2	- The composite film is prepared with transition metal oxides (e.g. Fe_2O_3 or CuO) - less expensive than Pt. - In combination with an air bleed, it is possible to raise the CO tolerance of a Pt/C to the same level as a PtRu/C alloy. - The design is simple and there is no need for additional hardware.	- Careful control for the oxidant bleed is required. - Limited studies about the stability of the catalysts.	- The cells can tolerate up 500 ppm CO/H_2, if the air-bleed limit is increased to 6%.	183, 184
	Catalyst sheet in front of the anode	5000 ppm CO/H_2	- The catalyst-sheet does not significantly hinder the gas transport to the anode or cause additional Ohmic losses. - The reformate can be directly introduced into the cells.	- Careful control for the oxidant bleed is required.		185
Pulsed heating	N.A.	1000 ppm CO/H_2	- The temperature of the membrane is not affected, maintaining its conductive properties. - The performance was four times higher. - The removal of CO is done in short periods of time.	- The implementation of the technique affects the structure of each of the cells.		155

Table 6. In-operando mitigation strategies for CO poisoning in PEMFC (continuation)

Mitigation strategy	Subdivision	Stream with the highest reported CO content in the anode	Advantages	Disadvantages	Comments	References
Pressure swing	N.A.	1000 ppm CO/H_2	The amount of oxidant is significantly reduced in comparison with conventional external oxidant bleeding. - High efficiency.	- Extensive control needed.		155
Break-in procedure and $KMnO_4$ treatment	N.A.	100 ppm CO/H_2	- Highly efficient, simple and applicable to larger stacks.	- Interrupted operation of fuel cell.	- The break-in procedure is predominant at higher operating temperatures. - The combined procedure of break-in and $KMnO_4$ solution regenerates 90% of the performance of the cells.	170
Triode operation	N.A.	760 ppm CO / 4.05% CO_2 / 4.6% H_2 / 3.8% N_2 / He	- Operation allows potential differences not accessible in normal operation.	- The three electrodes work in corrosion mode. - Some power is compromised in the operation of the auxiliary electrode.	- Triode operation has been used in SOFC to improve their performance in the presence of H_2S. - Also used in electrolysers and batteries.	186-190
Periodic variation in the fuel supply	Cyclic injection of pure H_2	72 ppm CO/H_2	- The endurance of the membrane is maintained as there are no major voltage excursions.	- Exhaustive control of CO content needed. - Not effective against irreversibly adsorbed contaminants. - The recovery time can be very long.	- The cell was completely recovered after 15 min of pure H_2, after the exposure to 100 ppm CO/H_2.	191, 192
	Periodic fuel starvation	75% H_2 /25% CO_2/100 ppm CO	- The application of different fuel-free fluid, from nitrogen, to water, a cooler or the recirculation from the cathode outlet.	- Careful cell monitoring required to ensure fuel starvation effects do not become extreme and affect the durability of the fuel cell.		192

Table 7. In-operando mitigation strategies for CO poisoning in PEMFC (continuation)

Mitigation strategy	Subdivision	Stream with the highest reported CO content in the anode	Advantages	Disadvantages	Comments	References
Pulsed oxidation or pulsing technique	Current pulses	3% CO/H_2	- As the removal of CO is done in a short period of time, the anode potential is maintained in the hydrogen oxidation region rather than at the CO oxidation potential. - The frequency of the pulses can be adjusted to different concentrations of CO. - No additional energy needed apart from the trigger device.	- Under short-circuit conditions, the anode potential might reach values above the thermodynamic stability limit, degrading its catalyst activity. - The use in stacks requires rigorous control of each of the cell's potentials. - The operation of the cells is interrupted during the operation.	- The use of a power converter to modulate the application of the pulses can increase the power of the cell by 50% in the presence of 500 ppm CO/H_2 and extend the fuel cell lifetime without reducing the output power.	45, 154, 193-196
	Negative potential pulses	50 ppm CO/H_2	- Rapid and with less experimental requirements than under the conventional oxidant bleeding. - Increase of up to 500% of the voltage output.	- Takes a significant amount of power to apply negative pulses.		197, 198
Potential oscillations or self-oscillations	N.A.	1000 ppm CO/H_2	- No control system or any additional equipment needed. - Can be used as a back-up solution.	- Takes place under limited operating conditions (e.g. concentrations higher than 50 ppm CO/H_2).	- Current pulsing technique is more effective than "self-oxidation" in increasing CO tolerance.	45, 199

3.3.1 CO tolerant electrocatalysts

The development of electrocatalysts is an area of significant research for CO poisoning mitigation. Suitable catalysts for CO tolerance must exhibit high activity for the HOR and the lowest possible overpotential in the presence of CO.[200] It is necessary to maximize the oxidation of CO, and reduce the adsorption processes for the improvement of the CO tolerance.[200] This has been achieved by alloying Pt with Ru, for example. PtRu/C is considered as one of the most promising CO-tolerant electrocatalysts, and is the most commercially available.[201]

The bifunctional and the electronic mechanisms are well-accepted pathways that explain the increased tolerance to CO. These were first proposed from studies performed on PtRu catalysts and then expanded to other systems. The electronic or ligand effect considers the decrease of the Pt-CO bond strength by the addition of the additional alloying element. The platinum properties are modified by the electron donation or back-donation of ruthenium. The CO adsorption energy decreases reducing the CO coverage.[202, 203] The electronic modifications also affect the CO oxidation reaction rate. At lower potentials, the electronic mechanism predominates due to the diminishment of CO adsorption, and at higher overpotentials, the bifunctional mechanism takes place.[200]

The bifunctional mechanism was first referred to PtRu alloys,[204] and occurs over the formation of oxygen-containing species, such as OH, on oxophilic sites present on the second element at lower potentials than for Pt, allowing electro-oxidation of CO to CO_2[202]. The mechanism between the adsorption of CO and the formation OH follows the Langmuir-Hinshelwood (L-H) mechanism:[200]

$$\mathbf{Pt + CO \rightarrow Pt - (CO)_{ads}} \quad (14)$$

$$\mathbf{M + H_2O \rightarrow M - OH + e^- + H^+} \quad (15)$$

$$\mathbf{M - OH + Pt - CO \rightarrow Pt + M + CO_2 + e^- + H^+} \quad (16)$$

Different electrocatalysts have been developed since. The structures are covered in several reviews.[69, 151, 152, 200, 205-208] Figure **27** presents the different classes of Pt-based catalysts for fuel cells,[208] although the non-platinum structures are of great interest due to the scarcity and the high costs of platinum.[209] Some representative examples from the vaste array of electro-catalysts are presented next.

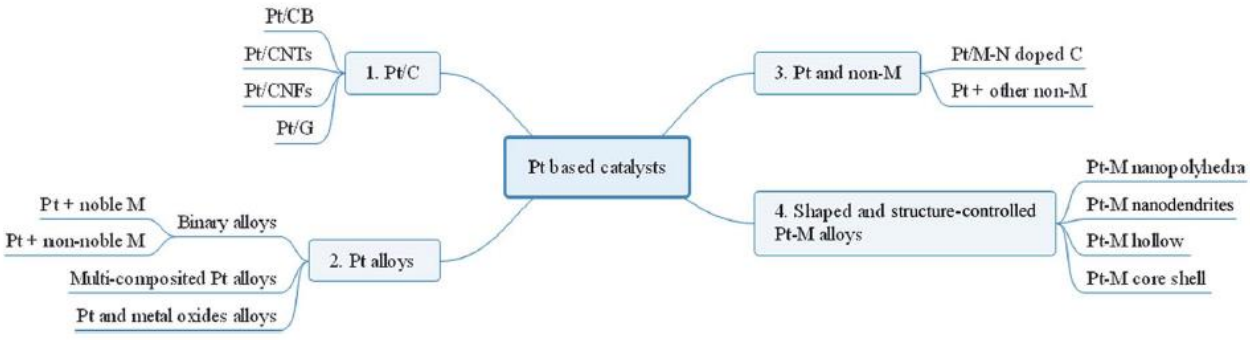

Figure 27. Representative classes of Pt-based catalysts for fuel cells. Reproduced with permission.[208] Copyright Royal Society of Chemistry, 2019

Ehteshami *et al.* compared the performance of a series of binary and ternary Pt-based catalysts (Figure **28**) and studied the relationship between the electronic properties of the catalysts and their tolerance to CO and CO_2. PtMo/C presented the highest CO tolerance due to the formation of well-dispersed oxy-hydroxides on the surface and to the turn-over of the Mo (IV/VI) redox couple, followed by PtCoMo/C, PtRuMo/C, PtRuPb/C, PtRu/C, PtCo/C, PtFe/C, PtNi/C and Pt/C. Although PtCoMo/C presented a higher CO oxidation onset potential than PtMo/C, this ternary electro-catalyst presented a higher tolerance to CO_2 by the added ligand effect due to the presence of Co, making it more suitable for the operation with reformate.[209]

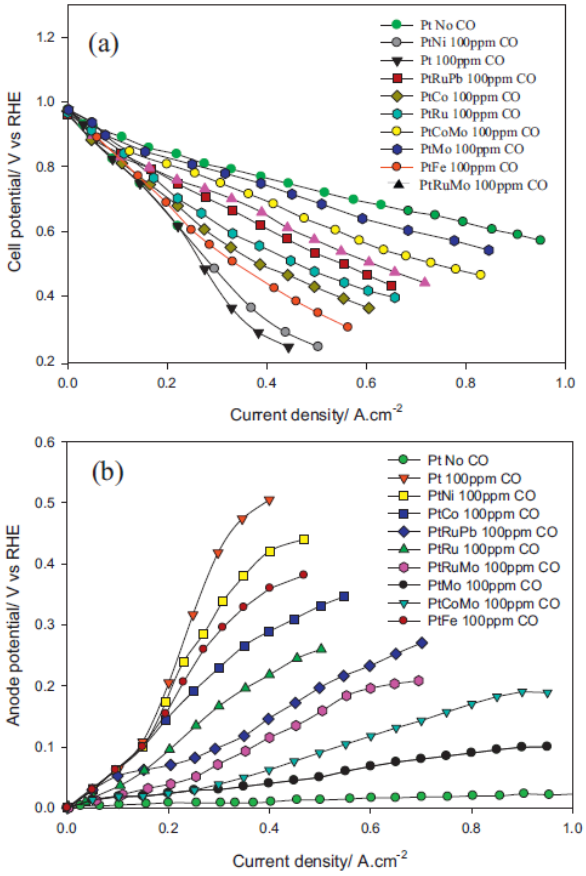

Figure 28. Comparison of the performance of different catalysts (Pt-M (M=Ru, Mo, Fe, Co, Ni), PtRuMo/C, PtCoMo/C, PtRuPb/C) in a H_2/O_2 PEM fuel cell system operating in the presence of 100 ppm CO/H_2. a) polarization curves and b) anodic overpotentials. Reproduced with permission.[209] Copyright 2013, Elsevier.

Some features have a direct impact on the catalyst efficiency and CO tolerance, including the type, composition and atomic ratios of the added elements. The synthesis method is also an important research area as the structure, morphology and size distribution of the catalysts rely on the process chosen.[151] For instance, Narischat *et al.* evaluated the effect of different porous structures of carbon support for Pt_2Ru_3 catalysts. The supports were prepared from resorcinol-formaldehyde carbon gels, varying the resorcinol to catalyst ratio (R/C). The highest tolerance was found to be related to the largest volume of mesoporous, due to a higher diffusivity. A cell using Pt_2Ru_3/RC1000ac58 (R/C=1000) presented a voltage decrease of 0.132 V at 0.2 A cm^{-2} in the presence of 2000 ppm CO/H_2.[157]

A catalyst class of interest is the core-shell structures due to the reduction of platinum utilisation. Some reports have also shown them to be more stable and catalytically more active than the alloy structures.[151] Most recent studies on the CO tolerance of core-shell catalysts include the synthesis of PtRu/PtNi/C with PtRu alloy surface and PtNi alloy core. The PtRu/PtNi/C catalyst presented a higher CO tolerance when compared to PtNi/C and PtNi-Ru/C in a PEMFC cell test in the presence of 30 ppm CO/H_2.[210]

Another novel catalyst studied is AuPt-prGO, a partially reduced graphene oxide sheet, incorporated with gold and platinum nanoparticles, presented by Isseroff *et al*. This material was applied to the electrodes and the membrane of a cell, showing a complete tolerance to 1000 ppm CO/H_2.[211]

As for the development of non-platinum electro-catalysts, a variety of tungsten carbide (WC) produced from different routes were tested in the presence of 1% CO/H_2 carbon catalyst in half-cell tests. The reduction in the current density due to the presence of CO was less than 6%, showing the weak adsorption of CO in catalyst sites.[158] Although these materials have shown a high CO tolerance, they present a low activity for HOR and are not convenient for commercial use.[159] More recently, Li *et al.* reported the synthesis of Ir-V-Mo/C catalysts. The ternary 40%Ir-10%V-10%Mo/C (in weight) presented a 26.4% higher power density than a conventional 40%Pt/C catalyst in a H_2/air system, and a superior tolerance to 10 ppm CO/H_2, due presumably to the bifunctional mechanism.[159]

Despite the progress made in the electro-catalysts area, there is room for improvement. At present, the research is concentrated in the development of CO-tolerant electrocatalysts more active and stable. For instance, the anode materials synthetized so far degrade under fuel cell operating conditions, due to leach out of the incorporated ions.[151] In the case of PtRu alloys, the anodic dissolution of ruthenium is favourable at potentials of 0.5 V vs RHE, leading to the loss of catalytic activity. Moreover, the dissolved ruthenium provokes the poisoning of the cathode due to its crossover, and the deterioration of the membrane properties.[154]

3.3.2 High-temperature fuel cells

As mentioned, CO poisoning is very temperature dependent. At higher temperatures, the hydrogen adsorption is less exothermic than the CO adsorption, the H_2 adsorption is favoured at higher temperatures, diminishing the coverage by CO and increasing the H_2 oxidation rate. The development of polymer membranes capable of operating at elevated temperatures opened up the possibility of high-temperature PEM fuel cells (HT-PEMFC).[161] HT-PEMFCs operate between 150 °C and 200 °C and are much more resistant to CO poisoning than conventional PEMFCs operating <80 °C. Figure 29 presents the effects of the operation of HT-PEMFC at different concentrations of CO.

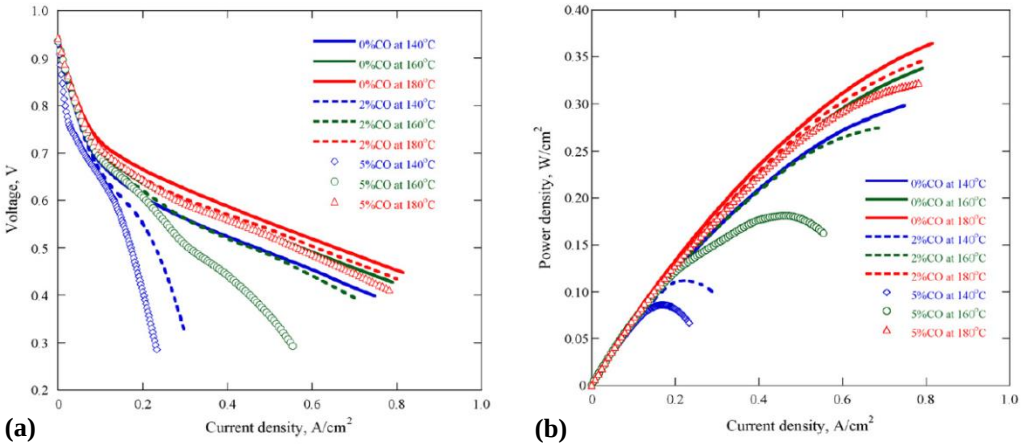

Figure 29 Effects of the temperature with a PBI-based PEMFC with different concentrations of CO: (a) polarization curves, (b) power density curves. Reproduced with permission.[161] Copyright 2009, Elsevier.

Another characteristic of this operation is the simplification of the water management problems that conventional PEMFC present. As the water is present only as vapour above 100 °C, flooding is not an issue. Nevertheless, the membrane is susceptible to lose ion conductivity due to dehydration.[161, 162] Additionally, a corrosion mechanism can be activated due to the high operating temperatures.[168]

Different membranes have been developed for high-temperature operation, such as inorganic-organic composite membranes, sulfonated hydrocarbon polymers and acid-base polymer membranes. The acid-base polymer membrane polybenzimidazole (PBI) doped with phosphoric acid (PA) has received much attention.[162] This membrane alone possesses a very low proton conductivity; however, the addition of PA increases it from 10^{-9} mS cm^{-1} to 0.1 S cm^{-1} at 150 °C.[212] At the same time, the addition of PA entails the blockage of the catalyst, especially on the cathode, limiting the oxygen reduction.[162]

HT-PEMFCs allow the use of direct reformate, containing 3% of CO,[163] and up to 5% of CO.[161] There is no need for other processes such as PSA, PROX or SMET, obtaining a simpler and more economical system (Figure 30).[162] Additionally, it is possible to integrate HT-PEMFCs into the fuel processing unit by recovering the heat from the cells and using it to service system requirements.[162, 212, 213] Moreover, it is also possible to mitigate the contamination by H_2S through this technique.[167] Liu *et al.* (2016) presented a comprehensive review of HT-PEMFCs for their use in auxiliary power units (APU).[214]

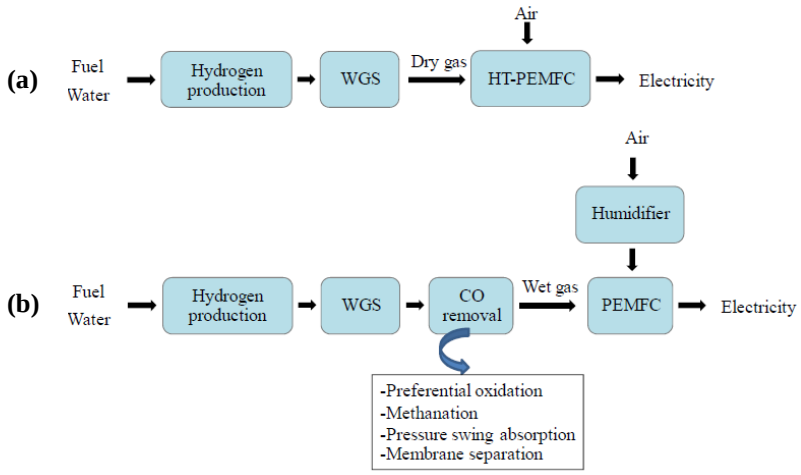

Figure 30 Comparison between (a) a conventional PEMFC system and (b) a HT-PEMFC. Reproduced with permission.[162] Copyright 2015, Elsevier.

3.3.3 Oxidant bleeding

Oxidant bleeding leads to the enhancement of the oxidation of CO to CO_2 through low levels of oxygen or oxygen-evolving/containing species, such as air or hydrogen peroxide. Sugiyama *et al.* (2019) deducted the energy profile of the CO oxidation by O_2 on Pt(111) surface, presented in Figure 31, where two pathways for the CO_2 formation are shown: (i) via O_2 dissociation, and (ii) via the OC-COO complex. The rate determining step via the O_2 dissociation corresponds to the generation and desorption of CO_2 (second step), while via the OC-COO complex the formation of this species is the rate determining step (first step).[215]

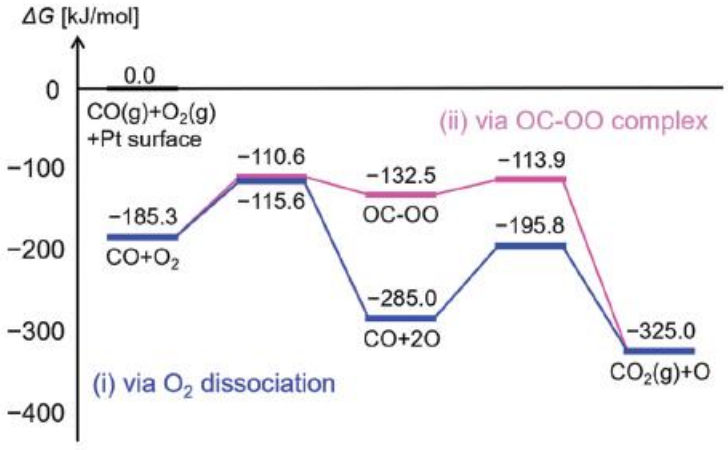

Figure 31. Energy profile of the CO oxidation by O_2 on Pt (111) obtained by the lowest conformer to single transition state (LC-TS) model at T = 300 K. The values of energy are relative free energies to the total energy of CO(g), O_2(g) and the Pt(111) surface. Reproduced with permission.[215] Copyright 2019, Royal Society of Chemistry.

This strategy was first introduced by Gottesfeld and Pafford (1988) who demonstrated that a concentration of 2-5% O_2/H_2 in the anode stream was enough to completely mitigate the effects of a concentration of 100 ppm CO at 80 °C.[55] The technique was quickly deployed and became one of the most studied. The variations over the introduction of the oxidant in the anode are presented next.

3.3.3.1 External bleeding

The external oxidant bleeding technique involves introducing the oxidant, usually air, into the fuel stream. The oxygen is adsorbed onto CO-free Pt catalyst sites, and then the surface reaction between Pt-CO and Pt-O takes place to form CO_2. This gas-phase catalytic oxidation reduces the CO coverage on the catalyst surface and increases the hydrogen electro-oxidation activity.[152] Roughly one out of every 400 O_2 molecules participates in the oxidation of CO.[216] The remaining oxygen chemically combusts with hydrogen.[217] Studies have summarized the different experimental conditions under which the CO poisoning has been evaluated.[169, 172] Figure 32 shows how current density is affected by cell exposure to different levels of air bleeding.[169]

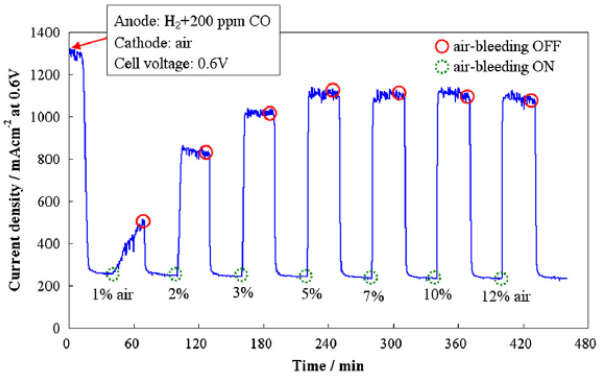

Figure 32. Evaluation of various levels of air bleeding on the current density of a fuel cell exposed to 200 ppm CO, operated at 0.6 V / 65 °C. Reproduced with permission.[169] Copyright 2013, Elsevier.

Cell potential losses due to CO poisoning can be mitigated by this technique, and recently it has been proven that low concentrations of H_2S can be mitigated through air bleeding.[160] However, there are significant drawbacks regarding anode lifetime due to the temperature increase caused by internal hydrogen combustion with oxygen, which is highly exothermic (Reaction 17). The temperature provokes the sintering of the catalyst that reduces the number of active sites.[152]

$$\mathbf{H_2 + \frac{1}{2}O_2 \leftrightarrow H_2O} \qquad \mathbf{\Delta H = -251\ kJ\ mol^{-1}} \qquad (17)$$

An additional drawback is the degradation of the membrane after extended periods of operation, due to the formation of hydrogen peroxide (H_2O_2).[171] Ralph *et al.* reported the appearance of pin-holes, leading to cell failure, although the anode lifetime can be increased by reconfiguring the anode (Section 3.3.4).[152] Other disadvantages of this technique are the inefficiency associated with consumption of hydrogen and the need for careful control of the air feed.[193]

Recent studies evaluated the effect of temperature in the effect of air bleeding, showing a slower process at higher temperature.[218] Another study includes the proposition of a methodology to optimize the amount of air bleed through the evaluation of the distribution of the contamination over a novel segmented cell, and the analysis of the CO conversion to CO_2.[172] Hafttananian *et al.* (2016) developed a model that apart from predicting the operation and the poisoning of the cell, could enhance the oxygen bleed and diminish oxygen / hydrogen consumption by 63%.[219] Another study checked the long-term effects of this technique.[220]

3.3.3.2 H_2O_2 in the anode humidifier

The use of hydrogen peroxide in the humidification of water was also evaluated.[66, 153, 173] The H_2O_2 is heterogeneously decomposed into active oxygen that contributes to the oxidation of the adsorbed CO in the catalyst, having the same effect as an air bleed.[173] Bellows *et al.* (1998) found that a certain amount of H_2O_2 is catalytically decomposed by interaction with the metallic surfaces of the humidifier.[153] The approach has certain safety advantages over air bleed; however, it presents other disadvantages inherent to oxidant bleeding (Section 3.3.3.1), in particular the degradation of the membrane in the long term due to the formation of H_2O_2.[171] In short-time operation the technique has been found to perform effectively, with 5% H_2O_2 in the deionized water of a humidifier completely avoiding the detrimental effects of 100 ppm CO in the anode hydrogen feed.[66]

3.3.3.3 Internal air bled

The carbon monoxide poisoning can also be mitigated by permeated oxygen coming from the cathode, which allows the heterogeneous oxidation of CO at the anode. This process is known as internal air bleed.[174] Wang *et al.* (2009) studied its effects on a Pt-Ru/C anode by increasing the cathode backpressure and the use of ultra-thin membranes ($\leq$ 25 μm) for a CO concentration of 50 ppm.[174] Sapountzi *et al.* (2007) also reported an increase in the Faradaic efficiency by 2.5 in the presence of 2400 ppm CO (0.24% CO/12.82% CO_2/ 12.84% H_2/12.18% N_2/ 61.92% He).[149] The main disadvantage of this approach is that use of a thin membrane can also lead to CO cross-over from the anode to the cathode, which can degrade the cathode electrocatalyst and decrease membrane proton conductivity.[34] The formation of H_2O_2 from the diffused O_2 to the anode is also pernicious, as it provokes the degradation of the membrane in the extended hours of operation.[171]

3.3.4 Reconfiguration of the anode

The modification of the anode structure has also been evaluated. The different approaches followed are presented next. These comprehend the inclusion of additional layers of different composition to the catalyst or diffusion layer, and/or the spread of new particles in the diffusion layer. The research about these methods is limited and certain concerns about

their applicability, such as durability and costs, remain unsolved. However, when these structures are used in conjunction with an oxidant bleeding, these avoid the heating problems that degrade the performance of the cells in the long term.

3.3.4.1 Bilayer anode structure

Composite electrodes with different layers have been proposed by Johnson Matthey and Ballard Power Systems.[221] As hydrogen diffuses faster than CO, the inner catalyst layers of the composite electrodes have a higher loading of platinum to sustain the hydrogen oxidation reaction (HOR). The CO reacts in the outer layers, where bespoke CO oxidation catalysts are used. The layers can be designed with different electrocatalyst components, contents and pore distribution. This method allows the total amount of catalyst used to be reduced without any loss of performance.[175, 176] The decrease in the anodic overpotential was confirmed by a modeling study presented by Janssen *et al*. (2004), where single layers and bilayer structures were compared.[178]

Different catalysts layers prepared by different methods have been studied. Yu *et al*. (2002) proposed two layers of catalysts; a hydrophilic Pt/C inner-layer (0.02 mg cm^{-2} Pt) prepared by the transfer method,[222] and a PtRu/C (0.28 mg cm^{-2} Pt/Ru) outer-layer composed by a thin carbon cloth,[223] to mitigate 50 ppm CO.[175] Another proposition was to use an outer layer composed of two nano-Ru layers prepared by magnetron sputtering deposition, followed by a Pt_{50}-Ru_{50} layer by screen-printing. A third layer (the inner layer) is composed of pure Pt and is prepared by direct-printing on the membrane. This structure presents a better performance in the presence of 50 ppm CO than a conventional Pt_{50}-Ru_{50} screen printed on GDL.[216]

The method of preparation was shown to affect the performance. The sputter deposition technique in the outer layer was found to double the CO tolerance (200 ppm CO vs 100 ppm CO) compared to conventional ink-based filters. It creates more sites upon which CO can be oxidized, using 40% less of Ru (0.080 vs 0.21 mg cm^{-2}). The different structures studied are presented in Figure 33.[177] The most efficient structure corresponds to a sputter-deposited Ru filter placed beside a Pt:Ru alloy (Figure 34).[177]

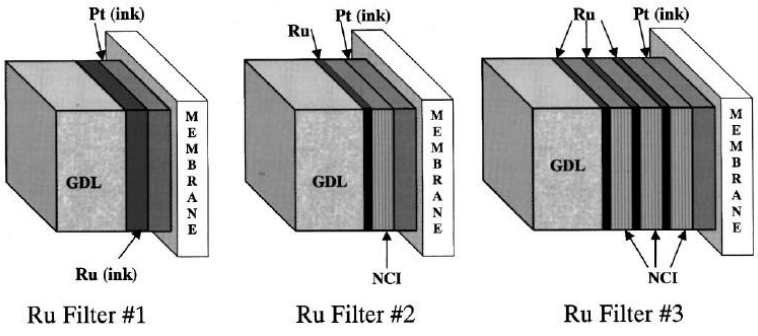

Figure 33. Structures of the Pt + Ru anodes studied. Filter 1: 0.08 mg cm^{-2} ink-based 20% Ru/C, Filter 2: Nafion-carbon ink (NCI) + 25 min (0.08 mg cm^{-2}) of sputter-deposited Ru, and Filter 3: NCI + 3 × (8.33 min of sputter-deposited Ru + NCI). The total Ru loading was 0.08 mg cm^{-2}. Reproduced with permission.[177] Copyright 2002, The Electrochemical Society, Inc.

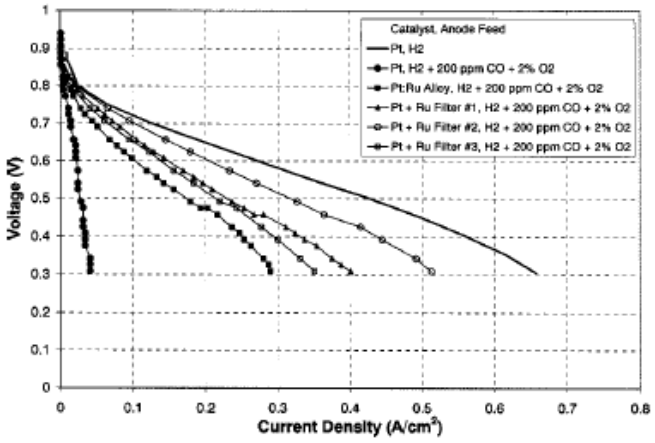

Figure 34. Performance comparison of the configurations of MEAs presented in Figure 33, under H_2 + 200 ppm CO + 2% O_2. P = 1 atm, T = 70 °C. Reproduced with permission.[177] Copyright 2002, The Electrochemical Society, Inc.

An additional advantage of the bilayer structure is that it can be used to mitigate CO_2 contamination[178] and the combined use with air bleeding extends the lifetime of the cell, as shown in Figure 35, where a reformate containing 70% H_2, 5% N_2, 25% CO_2 and 40 ppm CO was evaluated. 3% of air bleed was necessary to maintain the cell performance.[152]

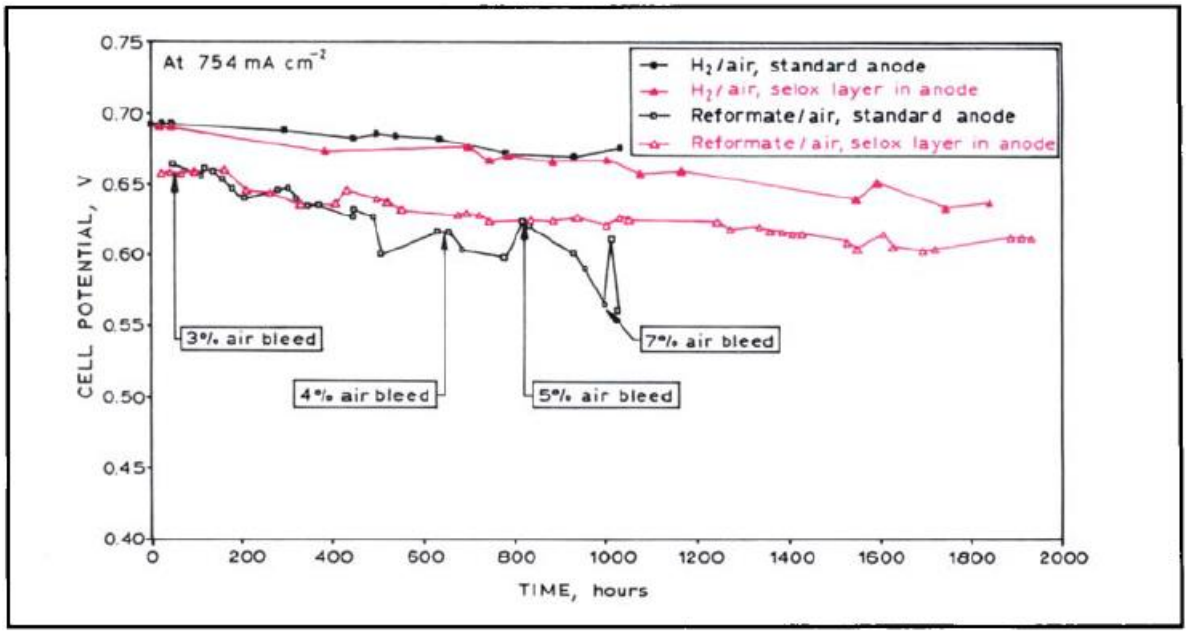

Figure 35. Durability study of a standard anode and a bilayer anode structure for hydrogen/air and reformate (70% hydrogen, 5% nitrogen, 25% CO_2, 40 ppm CO)/air operation at 754 mA cm^{-2} with an air bleed. The standard anode is composed of 20% Pt, 10%Ru/Vulcan XC72R at a loading of 0.25% mg Pt cm^{-2}. The bilayer structure includes an additional catalytic oxidation layer (selox layer) containing 20% Pt/Shawinigan carbon black at a loading of 0.1 mg Pt cm^{-2}.[152]

A bilayer structure conformed of an exterior layer of PtMo and an interior layer of PtRu was studied by Ball *et al.* The PtMo/PtRu electrode was tested in the presence of concentrations of CO as high as 5000 ppm CO/H_2, obtaining a good performance, even in the absence of an air bleed. In spite of the quantity of platinum used, the results obtained opened up the possibility of reducing the system required for the purification of the reformate.[179, 180]

3.3.4.2 Refined diffusion layer

Shi *et al*. (2007) placed Pt or Au particles in the diffusion layer by impregnation, to enhance the oxidation of CO with oxygen before the gas reaches the catalyst layer of the anode. This structure can mitigate 100 ppm CO together with 2% of oxygen bleed.[181] Santiago *et al*. (2005) studied the modification of the diffusion layer, by applying filtering layers (Ru/C or RuO_xH_y/C) on the diffusion layer and evaluated their performance in the presence of 100 ppm CO/H_2.[182]

3.3.4.3 Complementary composite film coating

Uribe *et al*. (2004) placed a thin film composite layer in addition to the gas diffusion layer (GDL), containing an inexpensive non-noble metal based materials. The MEA is prepared by brush painting an ink containing the non-noble metal on the anode carbon cloth, which is subsequently dried and sintered. As with the previous anode reconfigurations, the CO is oxidized with oxygen before entering the anode catalyst layer.[183]

A variety of metals were tested, from which the most effective in promoting the CO oxidation correspond to metals (or their oxides), that present at least two predominant low stable oxidation states (1 to 4).[183] Adcock *et al.* studied Fe, Co and Cu, from which the primary components in the composite were Fe_3O_4, Co_3O_4 and CuO, respectively. Figure 36 presents the voltage losses presented by these different complementary composite film coatings prepared and tested at 80 °C. The combined use of a complementary composite film coating and an air bleed (6%) enhance the tolerance of the cells to a concentration up to 500 ppm CO/H_2.[184]

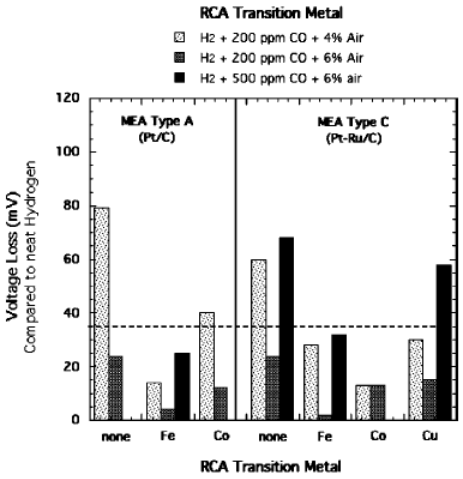

Figure 36. Voltage loss of the different anodes containing the complementary composite film coating at 0.5 A cm^{-2}. Fe major component: Fe_3O_4, Co major component: Co_3O_4 and Cu major component: CuO. The dotted line indicates maximum voltage loss considered as "full tolerance". Reproduced with permission.[184] Copyright 2005, The Electrochemical Society, Inc.

3.3.4.4 Catalyst sheet in front of the anode

Rohland and Plzak (1999) proposed a Ni-foam sheet filled with Au/Fe_2O_3 -catalyst powders. This catalyst sheet is placed in front of the Pt/Ru-C anode of a PEMFC, separated by carbon paper that provides the necessary electrical contact without compromising the gas transport (

Figure **37**(a)). The CO bonds created with Au are weaker than with Pt at 80 °C. Their strength is comparable to the CO bonds with Pt at 200 °C. The selective oxidation of CO is consequently increased in the Au-catalyst, providing a higher CO tolerance to the system. The catalyst sheet was tested simultaneously with an oxygen bleed, being able to mitigate 1000 ppm CO with 1% oxygen (

Figure **37**(b)).[185]

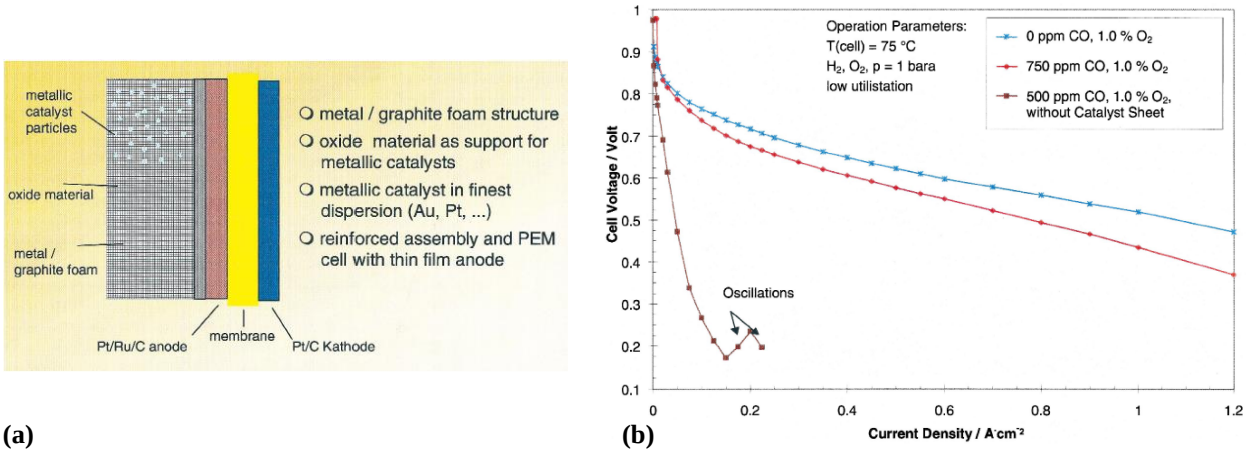

Figure 37. PEMFC with a catalyst sheet: (a) diagram of the components, (b) evaluation of the performance of the catalyst sheet together with an oxidant bleed. Reproduced with permission.[185] Copyright 1999, Elsevier.

3.3.5 Pulsed heating

A microheater device consisting of a stainless steel mesh was introduced in direct contact with the anode to locally increase the temperature, without affecting the temperature and the conductive properties of the membrane (Figure 38 (a)). The temperature of the anode was increased through heating pulses to recover the cell performance over-exposure to CO. The use of this recovery process allowed a performance four times higher than the poisoned case over the exposition to 1000 ppm CO/H_2.[155]

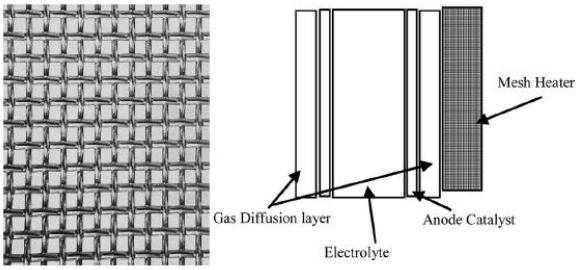

Figure 38. Application of heating pulses though the stainless steel mesh. Reproduced with permission.[155] Copyright 2009, The American Society of Mechanical Engineers.

3.3.6 Pressure swing

The pressure swing system was proposed by Guo *et al*. (2009). As shown in Figure 39(a), a fuel cell was divided into subunits, which were connected to a feed control valve. Through this valve it is possible to pull off the supply of hydrogen to specific units, producing a "vaccum". Unconsumed hydrogen from the anode outlet mixed with air or oxygen is then introduced to the starved cells.The amount of oxidant used is reduced compared to a typical air bleed, and the performance of the system is improved by a factor of four in the presence of 1000 ppm CO/H_2.[155]

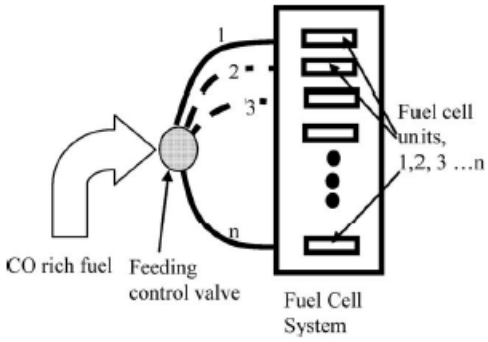

Figure 39 Diagram showing the disposition of the cells and the feeding control valve over the application of pressure swing. Reproduced with permission.[155] Copyright 2009, The American Society of Mechanical Engineers.

3.3.7 Combined break-in procedure and $KMnO_4$ treatment

Narayanan *et al*. (2017) proposed a regeneration process composed of a break-in procedure and the injection of a diluted solution of $KMnO_4$ in the anode. The break-in procedure consists of the application of lower and higher overpotentials

for a determined period, where the CO is oxidised to produce CO_2. In the presence of the $KMnO_4$ solution, the CO is also oxidised, this time by the nascent [O]. Figure 40 compares the influence of the break-in procedure and the $KMnO_4$ treatment on the catalyst activity at different temperatures. The combination of both treatments allows the regeneration of the catalyst by 90%.[170]

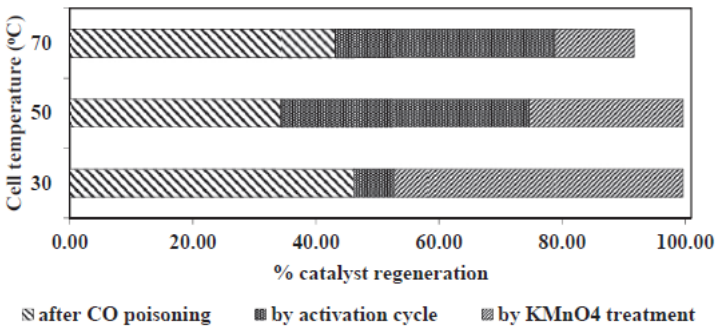

Figure 40. Regeneration of the catalyst for different temperatures through the break-in procedure (activation cycle) and the $KMnO_4$ solution treatment. Reproduced with permission.[170] Copyright 2017, Elsevier.

3.3.8 Triode operation

The triode operation consists of the addition of an auxiliary electrode to the fuel cell, in addition to the anode and the cathode, and in contact with the membrane (Figure 41). Two circuits are formed:

- The conventional fuel cell circuit between the anode and the cathode.
- An auxiliary circuit, between the auxiliary electrode and the cathode, working in parallel to the fuel cell and in electrolytic mode (I_{aux}<0 and ΔV_{aux}<0).

Over the operation, the potential difference between the auxiliary electrode and the cathode increases simultaneously the potential difference between the anode and the cathode. This allows the fuel cell to operate at potentials not accessible under normal operation (higher than 1.23 V), and thus, enhance its performance.[187, 188, 190] Figure 42 presents the performance of a cell exposed to 90 ppm CO/H_2 under triode operation.[190] In the presence of CO, the transport of protons from the auxiliary electrodes enhances the oxidation of CO, favouring the self-sustained potential oscillations.[187, 188] Katsaounis *et al.* (2005) explained the improvement of the performance of the cells under triode operation by the proton tunnelling mechanism, which increases the membrane conductivity.[224, 225]

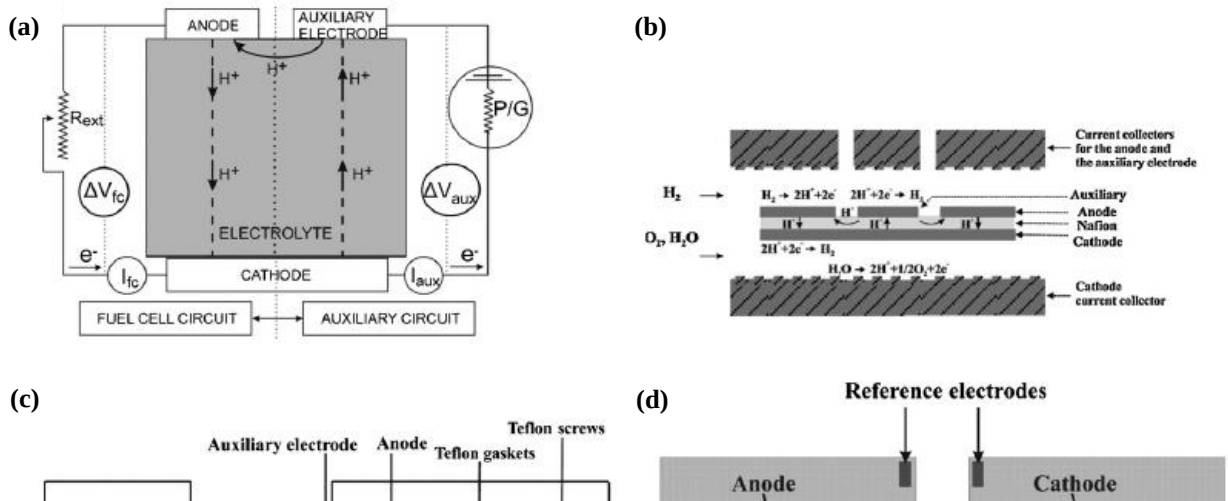

Figure 41. Triode operation system: a) Circuits involved and different current flow direction, b) reactions taking place, c) side-view of the system and d) electrodes layout as part of MEA. P/G: potentiostat-galvanostat. Reproduced with permission.[188] Copyright 2012, Elsevier.

.

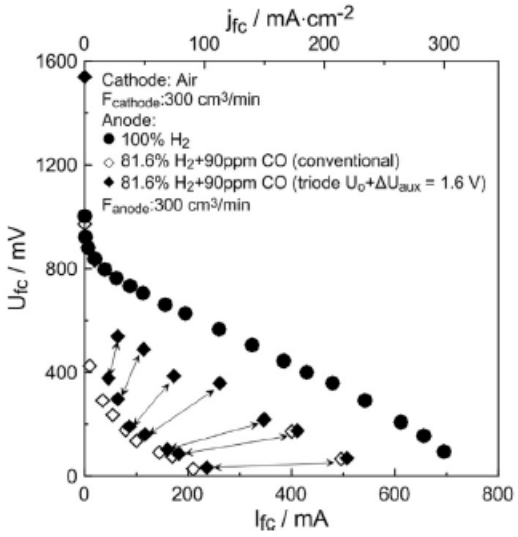

Figure 42. Polarization curves of a fuel cell exposed to pure H_2 and to 81.6% H_2 and 90 ppm CO /H_2. These are compared with the triode operation over the exposition to 81.6% H_2 and 90 ppm CO /H_2. The arrows over the triode operation represent self-sustained current or potential oscillations. Reproduced with permission.[190] Copyright 2017, Elsevier.

Another advantage is the use of less expensive materials[186, 224] and practical adaptation into stacks.[187, 188, 190] Among the disadvantages is the power consumption in the auxiliary circuit, and the corrosion-type mode under which the three electrodes, as reduction and oxidation reactions take place on their surface at the same time.[187, 188, 190]

Martino *et al.* (2017) developed a model based on the laws of Kirchhoff and the Nernst-Planck equation, and proposed a comb-type electrode geometry that reduced the resistance between the auxiliary electrode and anode or cathode. The new design was exposed to up to 120 ppm CO/H_2, increasing by 500% the power output compared to a fuel cell operation under the same concentration of CO.[190]

3.3.9 Periodic variation in the fuel supply

3.3.9.1 Cyclic injection of pure H_2

The reversibility of CO poisoning has been examined by different authors.[65, 69, 81, 95] Zhang *et al*. (2010 and 2011) showed that the adsorption of CO on Pt at 80 °C is reversible with a pure hydrogen purge, even when the Pt is exposed to high concentrations of CO.[226, 227] As such, the poisoning can be considered a transient phenomenon.[69]

Taking into account this property, Jimenez *et al*. (2005) proposed the cyclic feeding of hydrogen-containing CO, with the injection of pure H_2 streams. This operation allowed the desired cell voltage range to be maintained during operation on 72 ppm CO/H_2 (Figure 43). An advantage of this operation is that due to the relatively stable voltage, the lifetime of the cells is extended. However, careful monitoring and control of the feed gasses is required.[191]

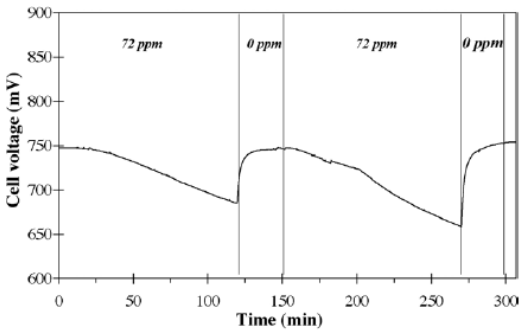

Figure 43 Cyclic injection of 72 ppm CO/H_2 and pure hydrogen. Reproduced with permission.[191] Copyright 2005, Elsevier.

3.3.9.2 Periodic fuel starvation

Hydrogen starvation occurs under extreme operating conditions (high currents, failure to supply adequate hydrogen to the anode), and results in an increase of the anode potential. The electric potential difference is consequently narrowed and even reversed.[228, 229] Wilkinson *et al.* (2000) presented the application of periodic starvation of fuel as a mitigation strategy against CO. In the presence of the contaminant, the increase of the anodic potential due to starvation is added to the rise due to the accumulation of CO in the catalyst, resulting in the oxidation of CO.[192]

Different set-ups presented, such as the periodic interruption of the fuel, or the periodic introduction of a fuel-free fluid, such as nitrogen, argon, helium and hydrocarbons into the anode. Other possible fuel-free fluids are liquid water or the cathode exhaust from the fuel cell. Another setup involves the application of a higher transient load, without the respective increase of the fuel flow. It was proposed that the starvation is applied in a portion of the anode while maintaining continuity in power supplied by the rest of the fuel cell.[192]

An important consideration is the parameters used to define the periods of fuel starvation and supply, as cell reversal is undesirable. A controller is used to vary the frequency and length of the pulses following a specific time set, or by monitoring the performance of the cell.[192] The reversal of the cell implies the consumption and not the supply of energy, the production of oxygen in the anode and of hydrogen in the cathode, and irreversible damage in the cell materials that affects the durability of the cell.[228] The technique has been evaluated in the presence of 75% H_2, 25% CO_2 and 10 ppm or 100 ppm CO.[192]

3.3.10 Pulsed oxidation or pulsing technique

3.3.10.1 Current pulsing

The current pulsing technique involves introducing periods of high load (high current) so that the anode potential increases and CO on the catalyst is oxidised to CO_2 (

Figure **44**).[193] The removal of CO from the Pt surface occurs in a short period (tens of milliseconds); thereby the anode potential is mostly in the hydrogen oxidation region rather than in the for CO oxidation potential.[32]

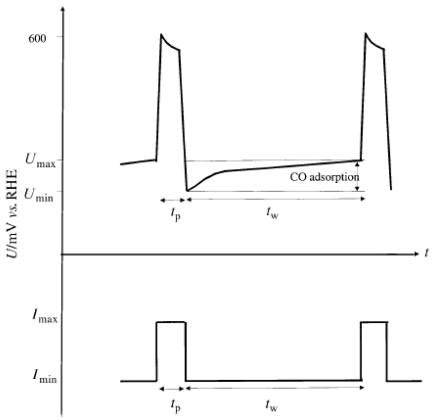

Figure 44. Pulsing technique description. The current is pulsed over the period t_P. t_W corresponds to the waiting time as CO builds up on the catalyst surface again. Reproduced with permission.[193] Copyright 2001, The Royal Society of Chemistry.

The pulse amplitude can be adjusted depending on the specific MEA, as the potential at which the CO oxidation occurs depends on the catalyst used. This can be determined through cyclic voltammetry. As for the pulse duration, some reports recommend keeping this constant regardless of the CO concentration in the feed.[193] Extending the pulse time unnecessarily long will reduce the fuel cell efficiency.[196] Rather, it is the frequency of the pulse that should be used as the key parameter to tune depending on the size of the electrode, flow rate and CO concentration of the anode feed.[193]

Studies with different CO concentrations have been performed, from 50 ppm to 3% CO/H_2,[32, 45, 193, 196, 230] with good results compared to the operation with pure H_2. In the case of 3% CO/H_2, a feedback control algorithm was used, using the current pulsing and the flow rate as control variables. 54% of the power obtained with pure H_2 was reached (Figure 45).[230] Another advance for the application of this technique is the model proposed by Ozdemir *et al.* (2016) that predicts the CO coverage and the CO-free surface over the application of the current pulsing technique in the presence of 10,000 ppm CO/H_2.[231]

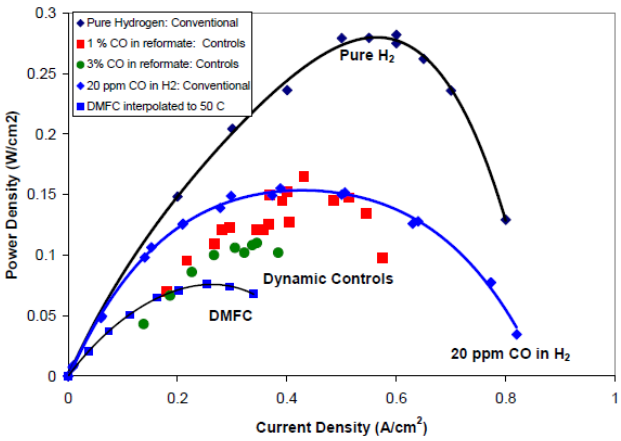

Figure 45. Power density obtained for a PEMFC with pure H_2 and 20 ppm CO/H_2 over a conventional operation, and with 1 and 3% CO/H_2 using a feedback control algorithm. Reproduced with permission.[230] Copyright 2008, The Electrochemical Society, Inc.

The pulsing technique presents several advantages as it allows the direct use of reformate gas without a significant loss of performance. Additionally, to carry out this technique, no external source of energy is necessary, apart from that required to trigger the pulsing event. As for the losses, these arise due to the low voltage (inefficient operation) during the pulse.[193]

On the other hand, long-term stability tests are needed for the catalysts used in this method,[193] such as the Pt dissolution and the loss of ECSA (electrochemical surface area). This constitutes the main reasons for the optimization of the pulses to reach a sufficiently high anode overpotential to oxidise CO, but not so much as to stress the electrode materials into degradation by dissolution, for example.[231]

While execution of this method with single cells is quite straight-forward, applying it to a stack is much more challenging as the balance of reactant distribution and resistances in the stack means that each cell is likely to behave differently during the pulse period. Therefore, the approach can only be relied upon in a conventional bipolar stack if rigorous control of the voltage of each cell in the stack can be achieved.[196] Adams *et al.* (2002) proposed a new device that allows each cell in the stack to be pulsed independently under controlled conditions. The Fuel Cell Health Manager (FCHM) is a microprocessor-based controller that has proved to be effective with 10,000 ppm CO.[32, 232, 233]

Another strategy to optimize the application of current pulses is the use of a power converter. For instance, a two-stage dc/dc power converter with a supercapacitor module was proposed by Woojin *et al*. (2004) to perform in a clean, fast and reliable manner the pulsing technique. It was possible to increase the power of the fuel cell by 50% in the presence of hydrogen fuel with 500 ppm CO. The diagram of the device and the performance studies are shown in

Figure 46.[194]

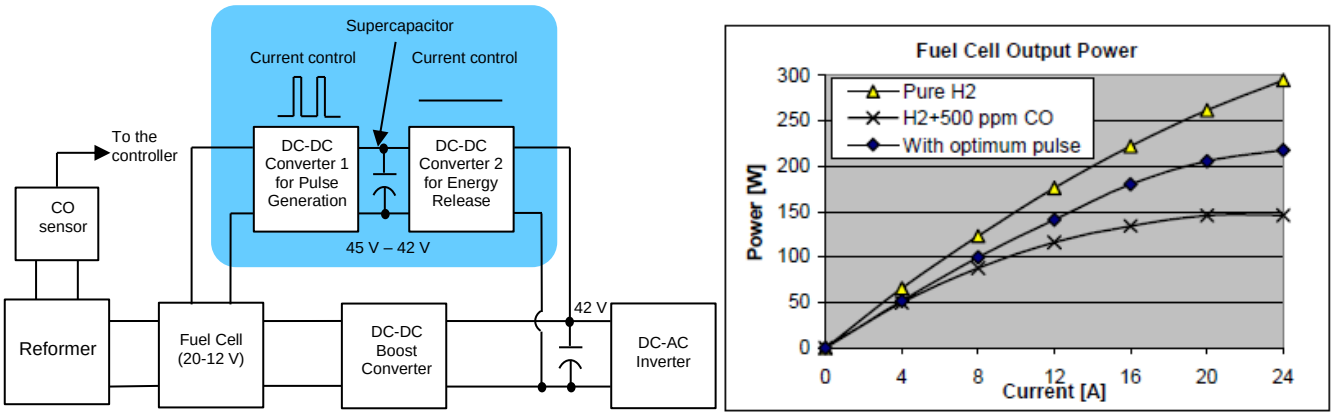

Figure 46. Optimization of the current pulsing through a power converter: (a) Diagram of the two-stage dc/dc power converter with a supercapacitor module, (b) comparison of the power output of a cell operating with pure H_2, 500 ppm CO/H_2 and 500 ppm CO/H_2 with current pulses. Reproduced with permission.[194] Copyright 2004, IEEE.

Palma *et al*. (2008 and 2017) proposed a different power converter able to modulate the current drawn from the stack. As is shown in Figure 47, instead of applying pulses of fixed magnitude, as in the conventional current pulsing technique, the pulses vary linearly with load current until full load. Figure 47 also presents the system, which has a boost converter in parallel with the reverse blocking diode placed at the output terminals of the fuel cell. It only operates for the duration of the pulses. The use of this device leads to reduced losses when operating at light loads. It also extends the lifetime of the fuel cell without reducing the output power.[195, 234]

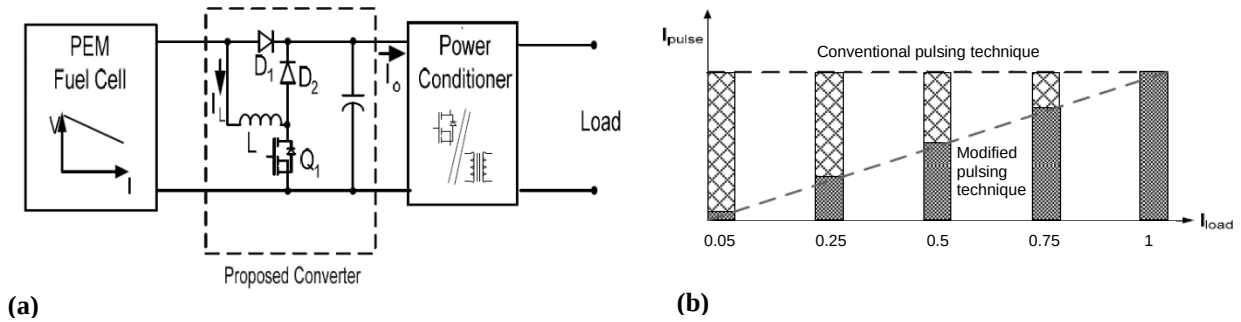

Figure 47. Power converter for the optimisation of the current pulsing technique: (a) Diagram of the power converter that includes a boost converter in parallel with the reverse blocking diode placed at the output terminals of the fuel cell, (b) comparison between the conventional pulsing technique and the modified pulsing technique used in the power converter. Reproduced with permission.[195] Copyright 2008, IEEE.

3.3.10.2 Negative potential pulses

Mao *et al*. (2000) were the first to propose the application of a reverse voltage for the regeneration of a single PEMFC in the presence of CO at the anode. During the negative pulse, water present at the anode is electrolyzed, producing oxygen that oxidises the carbon monoxide on the Pt surface.[198] The electrolysis reactions taking place are[197]

$$4H_2O + 4e^- \rightarrow 2H_2 + 4OH^- \quad (18)$$

$$2H_2O \rightarrow O_2 + 4H^+ + 4e^- \quad (19)$$

Wingelaar *et al*. (2007) studied the application of periodic negative voltages to regenerate a system composed of four cells fed in series, but electrically connected in pairs (the first two and the last two in parallel).[197] Although the application of negative voltage pulses requires a significant amount of power, it was possible to increase to up to 500% the voltage output of the system when exposed to 50 ppm CO/H_2. The electrical position of the individual cells in the stack determined their CO-tolerance and regeneration.[197] Other advantages found by Mao *et al*. (2000) were the rapid and more controllable application of this pulsing technique compared to oxidant bleeding.[198]

3.3.11 Potential oscillations or self-oscillations

The spontaneous potential oscillations over the CO poisoning mentioned in Section 1.2.2 can also be used as a mitigation strategy. As there is no need for any active control system or any additional equipment, the self-oxidation can be considered a passive back-up solution.[45] As previously mentioned, the oscillations occur under determined conditions. For instance, the concentration of CO has to be high enough for the self-oxidation to take place,[45] and a minimum current density is required.[199]

Figure 48 shows the effect of the self-oxidation in a CO-poisoned cell with 496 ppm CO. The catalyst used was Pt/Ru. The cell voltage drops until it reaches ~ 0.2 V, at which point the anode overpotential is large enough to cause oxidation of CO. Thomason *et al*. (2004) compared this method to the current pulsing technique. Both presented a similar efficiency in terms of the voltage produced and the CO tolerance (496 ppm). However, the voltage cell was above 0.60 V about 50% of the time, compared to 80% in the case of the pulsing technique. The pulsing technique also produced 13% more energy, and 13% more average power. Figure 48 presents a comparison of the two techniques in terms of the voltage.[45]

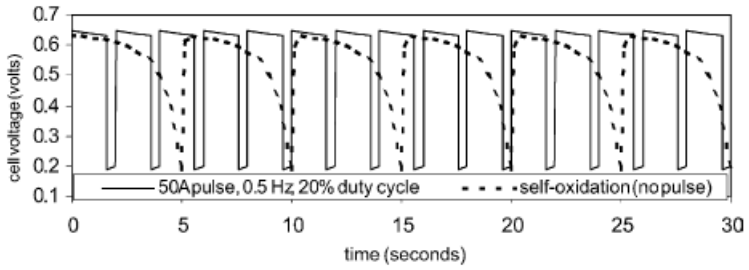

Figure 48. Variation of voltage over time of a cell exposed to 496 ppm CO/H_2. The constant cell current applied was at 20 A (0.4 A cm^{-2}). The pulse was 1.0 A cm^{-2} (50 A), 0.5 Hz, with a 20% duty cycle. Reproduced with permission.[45] Copyright 2004, Elsevier.

4. Critical discussion on mitigation strategies

An array of the mitigation strategies developed to counteract the pernicious effects of CO in PEMFC has been presented. Comparing the different technologies, it is possible to observe certain trends and elucidate the most promising techniques to be used in the future for each one of the categories where the strategies were divided.

Currently, 95% of the hydrogen generated worldwide is produced and used in the same location, as part of large industrial processes.[235] However, some expect hydrogen to be generated and purified on-board. This requires reformate pre-treatment technologies, that at present are part of large industrial processes, to evolve into more compact designs. An indication of this trend is the development of an ultrathin reformer incorporated to a high temperature PEMFC, presented by Avgouropoulos *et al.*[236] Another example would be the use of the Al_2O_3-supported Si_3N_4 membranes, which are already being used on-board.[141]

Membranes, in particular made of two-dimensional materials, are the most promising technology of the pre-treatment technologies presented. This is due in large part to the possibility of separating additional pernicious contaminants to the operation of PEMFC, such as CH_4 and CO_2. Membrane-based technologies also offer additional benefits such as low investment cost, facile operation, small footprint and easy maintenance.[113] Hence, this technology is also promising if adapted to on-board applications.

As mentioned, additional contaminants are present in the fuel, which depend on the nature of the generation of hydrogen. In the case of reformate, H_2S and NH_3 are also present apart from CO and cause degradation of the cells. Thus, the importance of the study of mixtures of contaminants and the development of mitigation strategies able to neutralize their combined effect. Examples of these mitigation strategies are the air bleed and the HT-PEMFC, able to mitigate both CO and H_2S.[160, 167] The deployment of these two strategies is expected to rise, in spite of their operational challenges.

Another area of interest is the development of electrocatalysts, as the scarcity and high costs of platinum represent one of the impediments for the commercialization of fuel cells.[151] Important progress has been reported in terms of CO tolerance and the reduction of platinum use. However, the stability of the catalyst structures, in particular of alloys, continues to be

a challenge. Although the catalyst tolerance to other contaminants such as H_2S has been explored,[237] the combined mitigation of CO, H_2S and other species has not been reported, showing a promising field of research.

Due to the catalyst limitations, other engineering and operational approaches have emerged from which, pulsed oxidation through current pulses presents the highest tolerance to CO. Cells have been tested in the presence of 3% CO/H_2.[230] Considering the CO content of the reformate after the WGS reaction of 1-2%,[14] this is a mitigation strategy that could contribute to the total reduction of the more complex purification stages. Moreover, no changes in the operating conditions, such as an increase in the temperature are needed, and no other reactant is added as in the oxidant bleeding technique. However, limitations still exist, such as the degradation of the catalyst and further development is needed.

5. Future research on CO poisoning

The research on CO poisoning in PEMFC is taking different directions. Firstly, new techniques are being developed to obtain more accurate measurements for a better understanding of the mechanisms of CO poisoning. For instance, Kaserer *et al*. (2013) took as a reference the localised reference electrode technology presented by Hinds *et al*. (2012) to study the poisoning in HT-PEMC.[238, 239] Another improvement is the rapid detection of the CO by in-line [240-242] and in-situ[243] sensors allowing the application of a mitigation strategy before the performance of the cell is degraded.

An increasing array of analytical techniques is being applied to understand the CO poisoning mechanism. Caldwell *et al*. (2015) applied Δμ adsorption near-edge spectroscopy (XANES) to reveal details of the binding-site for H, CO and biphosphate on the platinum anode catalyst that contributes to the better performance of HT-PEMFC in the presence of CO.[244] Another example is the use of the H_2-D_2 switch with Ar purge (HDSAP) method to study the effect of humidity on contamination.[226, 227]

Computational and modelling methods, often combined with experimental validation, are being more extensively applied to derive new insights and optimise mitigation techniques. For example, new methods for the interpretation of how the EIS response evolves over time due to the exposure of CO have been proposed. These include techniques such as real-time drift compensation, time course interpolation and Z-HIT refinement.[86, 97]

In the modelling of the poisoning process, models proposed present specific limitations, such as accounting for the homogeneity of contamination over the anode.[231] However, good agreement with experimental results is obtained over different stages of CO poisoning, which include an initial decrease in performance, pseudo-steady behaviour, and regeneration when exposed to pure hydrogen. These modelling studies have been reviewed and critically compared in the literature.[34, 231, 245]

The studies evaluating the effects of CO poisoning on the anode are extensive, with little research on the effects on other components of the cell. It is expected that the research on the impact on the cathode and the membrane, for instance, is extended, covering short and long-term effects. These studies could also be executed under the normal operation of the cell, and under harsh conditions prone to occur, such as cold-freezing conditions.

Another area of research concerns mixtures of contaminants, which corresponds to more plausible conditions of operation than a single contaminant. The nature of the contaminants depends on the hydrogen generation process and on the purification step. As new technologies are developed for the production of hydrogen, new contaminants are expected to emerge. The effects of many mixture combinations in operational fuel cell are unknown. For instance, it is known that methane (CH_4) is a contaminant produced from steam methane reforming and the purification by PSA.[246] Although its presence is rare, the combined effects with CO has not been studied.

As mentioned, the development of mitigation strategies against CO is a key factor for the deployment of PEMFCs, as the increase in the CO tolerance represents a reduction in the costs and volume of the hydrogen purification stages. The research for techniques that compel with these requirements without compromising the power generated by the fuel cells continues. Additional issues are their durability and complexity. CO tolerant electrocatalysts are the most researched area; however, a variety of new mitigation strategies has been proposed recently for their application over the hydrogen purification and separation in site and on board, and during the operation of the cells. Different approaches have been explored, from the variation of operating conditions, to the addition of new reactants in the fuel and the modification of the design of the cell.

Another approach towards the mitigation of CO poisoning is the application of dual-purpose redox processes. Designed for direct methanol fuel cells (DMFCs), the removal of CO is done by the injection of hexavalent chromium (Cr(VI)), a toxic and carcinogenic substance. The CO is used as a reducing agent for the Cr(VI) that is converted into Cr(III). The removal of CO and the conversion of Cr(VI) are done simultaneously.[247]

6. Conclusions

CO poisoning is an important area of research in PEM fuel cells as the performance and durability of these cells are significantly affected by it. A review of the mechanisms of contamination and its effects on the performance of the cells shows the complexity of the process as evidenced by the short and long-term degradation on the anode side, impact on the cathode side, and the heterogeneous spatial distribution of the contamination. In recent years, the development of more accurate techniques and advanced computational and modelling methods has contributed towards the discovery of new information about the phenomena. More research would elucidate a comprehensive profile of the poisoning and tolerance to CO.

Advancement in mitigation strategies that allow the reduction of the space and costs that the actual H_2 separation and purification processes represent is needed for the deployment of PEMFC. Over the last decade, an array of varied techniques has emerged at the ‘on site’ (pre-treatment of reformate) and ‘on board’ H_2 purification stages, and particularly over the operation of the cells. The development of CO-tolerant electro-catalysts continues to be the most studied; nevertheless, other approaches have been explored and shown to operate effectively with high CO tolerance.

7. Acknowledgements

The authors would like to acknowledge funding from the EPSRC (EP/L015277/1, EP/P009050/1, EP/M014371/1, EP/M009394/1, EP/M023508/1, EP/L015749/1, EP/N022971/1) for supporting fuel cell research in the Electrochemical Innovation Lab (EIL). PRS acknowledges the Royal Academy of Engineering for the Chair in Emerging Technologies and VFVL acknowledges the National Council of Science and Technology of Mexico (CONACYT).

8. References

1. A. S. Abdulkareem, A. S. Afolabi, N. Fungura, T. Mokrani and C. Mateescu, *Energy Sources, Part B: Economics, Planning, and Policy*, 2015, **10**, 404-411.
2. R. O'Hayre, S.-W. Cha, W. Colella and F. B. Prinz, *Fuel Cell Fundamentals*, John Wiley & Sons, New Jersey, Third Edition edn., 2016.
3. FuelCellToday, *Fuel Cell Electric Vehicles: The Road Ahead*, Royston, 2013.
4. USDOE, Types of Fuel Cells, http://energy.gov/eere/fuelcells/types-fuel-cells;, http://energy.gov/eere/fuelcells/types-fuel-cells, (accessed August, 2016).
5. D. Hart, J. Lewis, F. Lehner and M. Klippenstein, *Journal*, 2017.
6. USDOE, Fuel Cells, http://energy.gov/eere/fuelcells/fuel-cells;, http://energy.gov/eere/fuelcells/fuel-cells, (accessed August, 2016).
7. USDOE, in *The Fuel Cell Technologies Office Multi-Year Research, Development, and Demonstration Plan*, USDOE, 2016, ch. Fuel cells, pp. 3.4-1 -3.4-32.
8. B. M. Besancon, V. Hasanov, R. Imbault-Lastapis, R. Benesch, M. Barrio and M. J. Mølnvik, *International Journal of Hydrogen Energy*, 2009, **34**, 2350-2360.
9. D. D. Papadias, S. Ahmed, R. Kumar and F. Joseck, *International Journal of Hydrogen Energy*, 2009, **34**, 6021-6035.
10. BSI, *ISO 14687-3 Hydrogen fuel. Product specification. Proton exchange membrane (PEM) fuel cell applications for stationary appliances*, BSI Standards Limited, Switzerland, 2014.
11. BSI, *ISO 14687-2 Hydrogen fuel. Product specification. Proton exchange membrane (PEM) fuel cell applications for road vehicles*, BSI Standards Institution, Switzerland, 2012.
12. A. Basile, F. Dalena, J. Tong and T. N. Veziroğlu, *Journal*, 2017.
13. K. Liu, C. Song and V. Subramani, *Hydrogen and syngas production and purification technologies*, AIChE and John Wiley & Sons, Inc., Hoboken, New Jersey, 2010.

14. X. Cheng, Z. Shi, N. Glass, L. Zhang, J. Zhang, D. Song, Z. S. Liu, H. Wang and J. Shen, *Journal of Power Sources*, 2007, **165**, 739-756.
15. P. V. Snytnikov, M. M. Zyryanova and V. A. Sobyanin, *Top Catal*, 2016, **59**, 1394-1412.
16. B. Lakshmanan, W. Huang and J. W. Weidner, *Electrochemical and Solid-State Letters*, 2002, **5**, A267-A270.
17. T. M. Nenoff, R. J. Spontak and C. M. Aberg, *MRS Bull.*, 2006, **31**, 735-741.
18. S. Balasubramanian and J. W. Weidner, *Journal of The Electrochemical Society*, 2015, **162**, E231-E236.
19. X. Cheng, Z. Shi, N. Glass, L. Zhang, J. Zhang, D. Song, Z. S. Liu, H. Wang and J. Shen, *Journal of Power Sources*, 2007, 739-756.
20. J. W. Ha, J. Hyuck Jang, J. Hyoung Gil and S. H. Kim, *International Journal of Hydrogen Energy*, 2008, **33**, 2059-2063.
21. A. Godula-Jopek, in *Hydrogen Production*, Wiley-VCH Verlag GmbH & Co. KGaA, 2015, DOI: 10.1002/9783527676507.ch1, pp. 1-32.
22. J. Tafel, *Zeitschrift Fur Physikalische Chemie-Stochiometrie Und Verwandtschaftslehre*, 1905, **50**, 641-712.
23. J. Heyrovsky, *Recueil Des Travaux Chimiques Des Pays-Bas*, 1927, **46**, 582-585.
24. T. Erdey-Gruz and M. Volmer, *Z Phys. Chem A-Chem. Thermodyn. Kinet. Elektrochem. Eigensch.lehre*, 1930, **150**, 203-213.
25. H. Wang, X. Z. Yuan and H. Li, *PEM Fuel Cell Diagnostic Tools*, Taylor & Francis, 2011.
26. A. R. Kucernak and C. Zalitis, *The Journal of Physical Chemistry C*, 2016, **120**, 10721-10745.
27. W. Vogel, L. Lundquist, P. Ross and P. Stonehart, *Electrochimica Acta*, 1975, **20**, 79-93.
28. Wang, H. Wang, H. Li and X.-Z. Yuan, *PEM Fuel Cell Diagnostic Tools*, 2011.
29. S. Ye, T. Kondo, N. Hoshi, J. Inukai, S. Yoshimoto, M. Osawa and K. Itaya, *Electrochemistry*, 2009, **77**, 2-20.
30. N. M. Marković, B. N. Grgur and P. N. Ross, *Journal of Physical Chemistry B*, 1997, **101**, 5405-5413.
31. N. M. Marković and P. N. Ross, *Surface Science Reports*, 2002, **45**, 117-229.
32. W. A. Adams, J. Blair, K. R. Bullock and C. L. Gardner, *Journal of Power Sources*, 2005, **145**, 55-61.
33. A. Franco, *Polymer Electrolyte Fuel Cells: Science, Applications, and Challenges*, Pan Stanford Publishing, Stanford, 2013.
34. N. Zamel and X. Li, *Progress in Energy and Combustion Science*, 2011, **37**, 292-329.
35. P. Stonehart and P. N. Ross, *Catal. Rev.-Sci. Eng.*, 1975, **12**, 1-35.
36. S. Gilman, *The Journal of Physical Chemistry*, 1964, **68**, 70-80.
37. R. J. Bellows, E. P. Marucchi-Soos and D. T. Buckley, *Industrial & Engineering Chemistry Research*, 1996, **35**, 1235-1242.

38. H. Igarashi, T. Fujino and M. Watanabe, *Journal of Electroanalytical Chemistry*, 1995, **391**, 119-123.

39. H. A. Gasteiger, N. M. Markovic and P. N. Ross, *The Journal of Physical Chemistry*, 1995, **99**, 16757-16767.

40. D. C. Papageorgopoulos and F. A. de Bruijn, *Journal of The Electrochemical Society*, 2002, **149**, A140-A145.

41. M. Murthy, M. Esayian, A. Hobson, S. MacKenzie, W. K. Lee and J. W. Van Zee, *Journal of The Electrochemical Society*, 2001, **148**, A1141-A1147.

42. J. Zhang and R. Datta, *Journal of The Electrochemical Society*, 2002, **149**, A1423-A1431.

43. J. Zhang, J. D. Fehribach and R. Datta, *Journal of The Electrochemical Society*, 2004, **151**, A689-A697.

44. R. Hanke-Rauschenbach, M. Mangold and K. Sundmacher, *Journal*, 2011, **27**, 23.

45. A. H. Thomason, T. R. Lalk and A. J. Appleby, *Journal of Power Sources*, 2004, **135**, 204-211.

46. P. P. Lopes, E. A. Ticianelli and H. Varela, *Journal of Power Sources*, 2011, **196**, 84-89.

47. T. Kadyk, S. Kirsch, R. Hanke-Rauschenbach and K. Sundmacher, *Electrochimica Acta*, 2011, **56**, 10593-10602.

48. H. Lu, L. Rihko-Struckmann, R. Hanke-Rauschenbach and K. Sundmacher, *Physical Chemistry Chemical Physics*, 2011, **13**, 18179-18185.

49. A. Mota, P. P. Lopes, E. A. Ticianelli, E. R. Gonzalez and H. Varela, *Journal of The Electrochemical Society*, 2010, **157**, B1301-B1304.

50. R. Hanke-Rauschenbach, S. Kirsch, R. Kelling, C. Weinzierl and K. Sundmacher, *Journal of The Electrochemical Society*, 2010, **157**, B1521-B1528.

51. S. Kirsch, R. Hanke-Rauschenbach and K. Sundmacher, *Journal of The Electrochemical Society*, 2011, **158**, B44-B53.

52. S. Kirsch, Hanke-Rauschenbach, R., Stein, B., Kraume, R., Sundmacher, K., *Journal of The Electrochemical Society*, 2013, **160**, F436-F446.

53. P. Lopes, B. Batista, G. Saglietti, H. Varela and E. Ticianelli, *J Solid State Electrochem*, 2013, **17**, 1851-1859.

54. H. F. Oetjen, V. M. Schmidt, U. Stimming and F. Trila, *Journal of The Electrochemical Society*, 1996, **143**, 3838-3842.

55. S. Gottesfeld and J. Pafford, *Journal of The Electrochemical Society*, 1988, **135**, 2651-2652.

56. V. M. Schmidt, P. Bröckerhoff, B. Höhlein, R. Menzer and U. Stimming, *Journal of Power Sources*, 1994, **49**, 299-313.

57. A. Rodrigues, J. C. Amphlett, R. F. Mann, B. A. Peppley and P. R. Roberge, *Carbon monoxide poisoning of proton-exchange membrane fuel cells*, IEEE, IECEC-97 Proceedings of the Thirty-Second Intersociety Energy Conversion Engineering Conference, 1997.

58. H. P. Dhar, L. G. Christner and A. K. Kush, *Journal of The Electrochemical Society*, 1987, **134**, 3021-3026.

59. N. Zamel and X. Li, *International Journal of Hydrogen Energy*, 2008, **33**, 1335-1344.

60. J. Zhang, T. Thampan and R. Datta, *Journal of The Electrochemical Society*, 2002, **149**, A765-A772.

61. M. Murthy, M. Esayian, W. K. Lee and J. W. Van Zee, *Journal of The Electrochemical Society*, 2003, **150**, A29-A34.

62. T. Ioroi, K. Yasuda and Y. Miyazaki, *Physical Chemistry Chemical Physics*, 2002, **4**, 2337-2340.

63. F. Zhou, S. J. Andreasen, S. K. Kær and J. O. Park, *International Journal of Hydrogen Energy*, 2015, **40**, 14932-14941.

64. R. Jiang, H. R. Kunz and J. M. Fenton, *Journal of The Electrochemical Society*, 2005, **152**, A1329-A1340.

65. M. A. Díaz, A. Iranzo, F. Rosa, F. Isorna, E. López and J. P. Bolivar, *Energy*, 2015, **90**, 299-309.

66. J. Divisek, H. F. Oetjen, V. Peinecke, V. M. Schmidt and U. Stimming, *Electrochimica Acta*, 1998, **43**, 3811-3815.

67. F. A. de Bruijn, D. C. Papageorgopoulos, E. F. Sitters and G. J. M. Janssen, *Journal of Power Sources*, 2002, **110**, 117-124.

68. T. Gu, W.-K. Lee, J. W. Van Zee and M. Murthy, *Journal of The Electrochemical Society*, 2004, **151**, A2100-A2105.

69. J. J. Baschuk and X. Li, *International Journal of Energy Research*, 2001, **25**, 695-713.

70. T. Tingelöf, L. Hedström, N. Holmström, P. Alvfors and G. Lindbergh, *International Journal of Hydrogen Energy*, 2008, **33**, 2064-2072.

71. W.-M. Yan, H.-S. Chu, M.-X. Lu, F.-B. Weng, G.-B. Jung and C.-Y. Lee, *Journal of Power Sources*, 2009, **188**, 141-147.

72. T. Rockward, I. Urdampilleta, F. Uribe, E. L. Brosha, B. Pivovar and F. H. Garzon, *ECS Transactions*, 2007, **11**, 821-829.

73. W. Shi, B. Yi, M. Hou, F. Jing, H. Yu and P. Ming, *Journal of Power Sources*, 2007, **164**, 272-277.

74. X. Wang, Baker, P., Zhang, X., Garces, H. F., Bonville, L. J., Pasaogullari, U., Molter, T. M., *International Journal of Hydrogen Energy*, 2014, **39**, 19701-19713.

75. J. X. Wang, P. He, Y. Zhang and S. Ye, *ECS Transactions*, 2014, **64**, 121-127.

76. R. Borup, J. Meyers, B. Pivovar, Y. S. Kim, R. Mukundan, N. Garland, D. Myers, M. Wilson, F. Garzon, D. Wood, P. Zelenay, K. More, K. Stroh, T. Zawodzinski, J. Boncella, J. E. McGrath, M. Inaba, K. Miyatake, M. Hori, K. Ota, Z. Ogumi, S. Miyata, A. Nishikata, Z. Siroma, Y. Uchimoto, K. Yasuda, K. I. Kimijima and N. Iwashita, *Chemical Reviews*, 2007, **107**, 3904-3951.

77. S. Dorn, G. Bender, K. Bethune, M. Angelo and R. Rocheleau, *ECS Transactions*, 2008, **16**, 659-667.

78. M. Angelo, K. Bethune and R. Rocheleau, *ECS Transactions*, 2010, **28**, 169-181.

79. K. Kortsdottir, R. W. Lindström, T. Åkermark and G. Lindbergh, *Electrochimica Acta*, 2010, **55**, 7643-7651.

80. Z. Qi, C. He and A. Kaufman *Electrochemical and Solid-State Letters*, 2001, **4**, A204-A205.

81. Z. Qi, C. He and A. Kaufman *Journal of Power Sources*, 2002, **111**, 239-247.

82. T. V. Reshetenko, K. Bethune and R. Rocheleau, *Journal of Power Sources*, 2012, **218**, 412-423.

83. T. V. Reshetenko, K. Bethune, M. A. Rubio and R. Rocheleau, *Journal of Power Sources*, 2014, **269**, 344-362.

84. M. Angelo, G. Bender, S. Dorn, K. Bethune, T. Hossain, D. Posey, J. Gazda, A. Ghatak-roy and R. Rocheleau, *ECS Transactions*, 2008, **16**, 669-676.

85. I. Profatilova, P.-A. Jacques and S. Escribano, *Journal of The Electrochemical Society*, 2018, **165**, F3251-F3260.

86. N. Wagner and E. Gülzow, *Journal of Power Sources*, 2004, **127**, 341-347.

87. V. Parry, G. Berthomé, J.-C. Joud, O. Lemaire and A. A. Franco, *Journal of Power Sources*, 2011, **196**, 2530-2538.

88. S. Søndergaard, L. N. Cleemann, J. O. Jensen and N. J. Bjerrum, *International Journal of Hydrogen Energy*, 2017, **42**, 3309-3315.

89. A. A. Franco, M. Guinard, B. Barthe and O. Lemaire, *Electrochimica Acta*, 2009, **54**, 5267-5279.

90. M. Chandesris, L. Guetaz, P. Schott, M. Scohy and S. Escribano, *Journal of The Electrochemical Society*, 2018, **165**, F3290-F3306.

91. D. J. L. Brett, S. Atkins, N. P. Brandon, V. Vesovic, N. Vasileiadis and A. R. Kucernak, *Journal of Power Sources*, 2004, **133**, 205-213.

92. D. J. L. Brett, P. Aguiar, N. P. Brandon and A. R. Kucernak, *International Journal of Hydrogen Energy*, 2007, **32**, 863-871.

93. T. Murahashi, T. Mitsumoto and E. Nishiyama, *ECS Transactions*, 2009, **25**, 869-879.

94. M. Boaventura, H. Sander, K. A. Friedrich and A. Mendes, *Electrochimica Acta*, 2011, **56**, 9467-9475.

95. M. A. Rubio, A. Urquia and S. Dormido, *International Journal of Hydrogen Energy*, 2010, **35**, 2586-2590.

96. J.-M. Le Canut, R. M. Abouatallah and D. A. Harrington, 2006, **153**, A857-A864.

97. N. Wagner and M. Schulze, *Electrochimica Acta*, 2003, **48**, 3899-3907.

98. C. A. Schiller, F. Richter, E. Gulow and N. Wagner, *Physical Chemistry Chemical Physics*, 2001, **3**, 2113-2116.

99. N. Wagner and E. Gülzow, *Journal of Power Sources*, 2004, **127**, 341-347.

100. Y.-J. Leng, X. Wang and I. M. Hsing, *Journal of Electroanalytical Chemistry*, 2002, **528**, 145-152.

101. B. M. Besancon, V. Hasanov, R. Imbault-Lastapis, R. Benesch, M. Barrio and M. J. Molnvik, *International Journal of Hydrogen Energy*, 2009, 2350-2360.

102. G. J. Grashoff, C. E. Pilkington and C. W. Corti, *Platinum Metals Review*, 1983, **27**, 157-169.

103. N. A. Al-Mufachi, N. V. Rees and R. Steinberger-Wilkens, *Renewable and Sustainable Energy Reviews*, 2015, **47**, 540-551.

104. I. Uehara, in *Energy Carriers and Conversion Systems with Emphasis on Hydrogen* ed. T. Ohta, EOLSS Publications, Oxford, United Kingdom, 2009, vol. 1, pp. 268-282.

105. J. Zhang and R. Datta, *Journal of The Electrochemical Society*, 2005, **152**, A1180-A1187.

106. E. D. Park, D. Lee and H. C. Lee, *Catalysis Today*, 2009, **139**, 280-290.

107. J. J. Conde, M. Maroño and J. M. Sánchez-Hervás, *Separation & Purification Reviews*, 2017, **46**, 152-177.

108. X. Yang Chen, L. Xiao Wei, L. Deng, F. Yang and Z. Zhang, *A Review on the Metal Hydride Based Hydrogen Purification and Separation Technology*, 2013.

109. J. Zhu, J. Hou, A. Uliana, Y. Zhang, M. Tian and B. Van der Bruggen, *Journal of Materials Chemistry A*, 2018, **6**, 3773-3792.

110. Z. Ma, X. Zhao, Q. Tang and Z. Zhou, *International Journal of Hydrogen Energy*, 2014, **39**, 5037-5042.

111. K. D. Modibane, M. Williams, M. Lototskyy, M. W. Davids, Y. Klochko and B. G. Pollet, *International Journal of Hydrogen Energy*, 2013, **38**, 9800-9810.

112. E. H. Majlan, W. R. Wan Daud, S. E. Iyuke, A. B. Mohamad, A. A. H. Kadhum, A. W. Mohammad, M. S. Takriff and N. Bahaman, *International Journal of Hydrogen Energy*, 2009, **34**, 2771-2777.

113. P. Bernardo, E. Drioli and G. Golemme, *Industrial & Engineering Chemistry Research*, 2009, **48**, 4638-4663.

114. S. Adhikari and S. Fernando, *Industrial & Engineering Chemistry Research*, 2006, **45**, 875-881.

115. G. Liu, W. Jin and N. Xu, *Chemical Society Reviews*, 2015, **44**, 5016-5030.

116. Y. Li, Z. Zhou, P. Shen and Z. Chen, *Chemical Communications*, 2010, **46**, 3672-3674.

117. Y. Tao, Q. Xue, Z. Liu, M. Shan, C. Ling, T. Wu and X. Li, *ACS Applied Materials & Interfaces*, 2014, **6**, 8048-8058.

118. S. Wei, S. Zhou, Z. Wu, M. Wang, Z. Wang, W. Guo and X. Lu, *Applied Surface Science*, 2018, **441**, 631-638.

119. G. Li, Y. Li, H. Liu, Y. Guo, Y. Li and D. Zhu, *Chemical Communications*, 2010, **46**, 3256-3258.

120. Y. Jiao, A. Du, M. Hankel, Z. Zhu, V. Rudolph and S. C. Smith, *Chemical Communications*, 2011, **47**, 11843-11845.

121. S. W. Cranford and M. J. Buehler, *Nanoscale*, 2012, **4**, 4587-4593.

122. W.-h. Zhao, L.-f. Yuan and J.-l. Yang, *Chinese Journal of Chemical Physics*, 2012, **25**, 434-440.

123. Y. Jiao, A. Du, S. C. Smith, Z. Zhu and S. Z. Qiao, *Journal of Materials Chemistry A*, 2015, **3**, 6767-6771.

124. X. Tan, L. Kou, H. A. Tahini and S. C. Smith, *Molecular Simulation*, 2016, **42**, 573-579.

125. H. Zhang, X. He, M. Zhao, M. Zhang, L. Zhao, X. Feng and Y. Luo, *The Journal of Physical Chemistry C*, 2012, **116**, 16634-16638.

126. Y. Ji, H. Dong, H. Lin, L. Zhang, T. Hou and Y. Li, *RSC Adv.*, 2016, **6**, 52377-52383.

127. L. Zhu, Y. Jin, Q. Xue, X. Li, H. Zheng, T. Wu and C. Ling, *Journal of Materials Chemistry A*, 2016, **4**, 15015-15021.

128. J. Xu, S. Zhou, P. Sang, J. Li and L. J. J. o. M. S. Zhao, 2017, **52**, 10285-10293.

129. M. V. Lototskyy, I. Tolj, L. Pickering, C. Sita, F. Barbir and V. Yartys, *Progress in Natural Science: Materials International*, 2017, **27**, 3-20.

130. S. Miura, A. Fujisawa and M. Ishida, *International Journal of Hydrogen Energy*, 2012, **37**, 2794-2799.

131. S. Miura, A. Fujisawa, S. Tomekawa, Y. Taniguchi, N. Hanada and M. Ishida, *Journal of Alloys and Compounds*, 2013, **580**, S414-S417.

132. *U.S. Pat.*, 4,217,759, 1980.

133. S. Balasubramanian, C. E. Holland and J. W. Weidner, *ECS Transactions*, 2009, **25**, 1873-1880.

134. K. A. Perry, G. A. Eisman and B. C. Benicewicz, *Journal of Power Sources*, 2008, **177**, 478-484.

135. M. Thomassen, E. Sheridan and J. Kvello, *Journal of Natural Gas Science and Engineering*, 2010, **2**, 229-234.

136. H. K. Lee, H. Y. Choi, K. H. Choi, J. H. Park and T. H. Lee, *Journal of Power Sources*, 2004, **132**, 92-98.

137. C. Oettel, L. Rihko-Struckmann and K. Sundmacher, *International Journal of Hydrogen Energy*, 2012, **37**, 11759-11771.

138. C. Oettel, L. Rihko-Struckmann and K. Sundmacher, *International Journal of Hydrogen Energy*, 2012, **37**, 6635-6645.

139. C. L. Gardner and M. Ternan, *Journal of Power Sources*, 2007, **171**, 835-841.

140. C. Huang, R. Jiang, M. Elbaccouch, N. Muradov and J. M. Fenton, *Journal of Power Sources*, 2006, **162**, 563-571.

141. X. Liu, P. A. Christensen, S. M. Kelly, V. Rocher and K. Scott, *Membranes*, 2013, **3**, 406-414.

142. R. Hanke-Rauschenbach, C. Weinzierl, M. Krasnyk, L. Rihko-Struckmann, H. Lu and K. Sundmacher, *Journal of The Electrochemical Society*, 2009, **156**, B1267-B1275.

143. H. Lu, L. Rihko-Struckmann, R. Hanke-Rauschenbach and K. Sundmacher, *Electrochimica Acta*, 2009, **54**, 1184-1191.

144. P. Heidebrecht, R. Hanke-Rauschenbach, A. Jörke and K. Sundmacher, *Chemical Engineering Science*, 2012, **67**, 34-43.

145. S. Balasubramanian, C. E. Holland and J. W. Weidner, *Electrochemical and Solid-State Letters*, 2010, **13**, B5-B7.

146. *U.S. Pat.*, 3,475,302, 1969.

147. *U.S. Pat.*, 3,489,670, 1970.

148. S. A. Grigoriev, I. G. Shtatniy, P. Millet, V. I. Porembsky and V. N. Fateev, *International Journal of Hydrogen Energy*, 2011, **36**, 4148-4155.

149. F. Sapountzi, M. N. Tsampas and C. G. Vayenas, *Top Catal*, 2007, **44**, 461-468.

150. J. Zhang, PhD thesis, Worcester Polytechnic Institute, 2004.

151. S. M. M. Ehteshami and S. H. Chan, *Electrochimica Acta*, 2013, **93**, 334-345.

152. T. R. Ralph and M. P. Hogarth, *Platinum Metals Review*, 2002, **46**, 117-135.

153. R. J. Bellows, E. Marucchi Soos and R. P. Reynolds, *Electrochemical and Solid-State Letters*, 1998, **1**, 69-70.

154. Y. V. Tolmachev and O. A. Petrii, *J Solid State Electrochem*, 2017, **21**, 613-639.

155. S. M. Guo and A. B. M. Hasan, *Journal of Fuel Cell Science and Technology*, 2009, **6**, 6.

156. P. P. Lopes and E. A. Ticianelli, *Journal of Electroanalytical Chemistry*, 2010, **644**, 110-116.

157. N. Narischat, T. Takeguchi, T. Mori, S. Iwamura, I. Ogino, S. R. Mukai and W. Ueda, *International Journal of Hydrogen Energy*, 2016, **41**, 13697-13704.

158. D. R. McIntyre, G. T. Burstein and A. Vossen, *Journal of Power Sources*, 2002, **107**, 67-73.

159. B. Li, D. C. Higgins, D. Yang, R. Lin, Z. Yu and J. Ma, *International Journal of Hydrogen Energy*, 2012, **37**, 18843-18850.

160. T. Lopes, V. A. Paganin and E. R. Gonzalez, *Journal of Power Sources*, 2011, **196**, 6256-6263.

161. S. K. Das, A. Reis and K. J. Berry, *Journal of Power Sources*, 2009, **193**, 691-698.

162. S. Authayanun, K. Im-orb and A. Arpornwichanop, *Chinese Journal of Catalysis*, 2015, **36**, 473-483.

163. J. K. Kallitsis, M. Geormezi and S. G. Neophytides, *Polymer International*, 2009, **58**, 1226-1233.

164. M. Geormezi, V. Deimede, N. Gourdoupi, N. Triantafyllopoulos, S. Neophytides and J. K. Kallitsis, *Macromolecules*, 2008, **41**, 9051-9056.

165. A. Orfanidi, M. K. Daletou and S. G. Neophytides, *Electrochimica Acta*, 2017, **233**, 218-228.

166. K. Jiao, Y. Zhou, Q. Du, Y. Yin, S. Yu and X. Li, *Applied Energy*, 2013, **104**, 21-41.

167. A. Vassiliev, L. N. Cleemann, Q. Li and J. O. Jensen, 2016, **MA2016-02**, 2813.

168. B. Decoopman, R. Vincent, S. Rosini, G. Paganelli and P. X. Thivel, *Journal of Power Sources*, 2016, **324**, 492-498.

169. L.-Y. Sung, B.-J. Hwang, K.-L. Hsueh, W.-N. Su and C.-C. Yang, *Journal of Power Sources*, 2013, **242**, 264-272.

170. H. Narayanan and S. Basu, *International Journal of Hydrogen Energy*, 2017, **42**, 23814-23820.

171. M. Inaba, M. Sugishita, J. Wada, K. Matsuzawa, H. Yamada and A. Tasaka, *Journal of Power Sources*, 2008, **178**, 699-705.

172. L. C. Pérez, T. Rajala, J. Ihonen, P. Koski, J. M. Sousa and A. Mendes, *International Journal of Hydrogen Energy*, 2013, **38**, 16286-16299.

173. V. M. Schmidt, H. F. Oetjen and J. Divisek, *Journal of The Electrochemical Society*, 1997, **144**, L237-L238.

174. W. Wang, *Journal of Power Sources*, 2009, **191**, 400-406.

175. H. Yu, Z. Hou, B. Yi and Z. Lin, *Journal of Power Sources*, 2002, **105**, 52-57.

176. A. T. Haug, R. E. White, J. W. Weidner and W. Huang, *Journal of The Electrochemical Society*, 2002, **149**, A862-A867.

177. A. T. Haug, R. E. White, J. W. Weidner, W. Huang, S. Shi, N. Rana, S. Grunow, T. C. Stoner and A. E. Kaloyeros, *Journal of The Electrochemical Society*, 2002, **149**, A868-A872.

178. G. J. M. Janssen, M. P. de Heer and D. C. Papageorgopoulos, *Fuel Cells*, 2004, **4**, 169-174.

179. S. C. Ball and D. Thompsett, *MRS Proceedings*, 2002, **756**, FF5.1.

180. S. Ball, B. Theobald and D. Thompsett, 2004, **2004-21**, 206-212.

181. W. Shi, M. Hou, Z. Shao, J. Hu, Z. Hou, P. Ming and B. Yi, *Journal of Power Sources*, 2007, **174**, 164-169.

182. E. I. Santiago, V. A. Paganin, M. do Carmo, E. R. Gonzalez and E. A. Ticianelli, *Journal of Electroanalytical Chemistry*, 2005, **575**, 53-60.

183. F. A. Uribe, J. A. Valerio, F. H. Garzon and T. A. Zawodzinski, *Electrochemical and Solid-State Letters*, 2004, **7**, A376-A379.

184. P. A. Adcock, S. V. Pacheco, K. M. Norman and F. A. Uribe, *Journal of The Electrochemical Society*, 2005, **152**, A459-A466.

185. B. Rohland and V. Plzak, *Journal of Power Sources*, 1999, **84**, 183-186.

186. S. P. Balomenou, F. Sapountzi, D. Presvytes, M. Tsampas and C. G. Vayenas, *Solid State Ionics*, 2006, **177**, 2023-2027.

187. F. M. Sapountzi, S. C. Divane, M. N. Tsampas and C. G. Vayenas, *Electrochimica Acta*, 2011, **56**, 6966-6975.

188. M. N. Tsampas, F. M. Sapountzi, S. Divane, E. I. Papaioannou and C. G. Vayenas, *Solid State Ionics*, 2012, **225**, 272-276.

189. P. Caliandro, S. Diethelm and J. Van herle, *Fuel Cells*, 2017, **17**, 457-463.

190. E. Martino, G. Koilias, M. Athanasiou, A. Katsaounis, Y. Dimakopoulos, J. Tsamopoulos and C. G. Vayenas, *Electrochimica Acta*, 2017, **248**, 518-533.

191. S. Jiménez, J. Soler, R. X. Valenzuela and L. Daza, *Journal of Power Sources*, 2005, **151**, 69-73.

192. *U.S. Pat.*, 6,096,448, 2000.

193. L. P. L. Carrette, K. A. Friedrich, M. Huber and U. Stimming, *Physical Chemistry Chemical Physics*, 2001, **3**, 320-324.

194. C. Woojin, P. N. Enjeti and A. J. Appleby, 2004.

195. L. Palma and P. Enjeti, *2008 IEEE Power Electronics Specialists Conference*, 2008, 210-215.

196. C. G. Farrell, C. L. Gardner and M. Ternan, *Journal of Power Sources*, 2007, **171**, 282-293.

197. P. J. H. Wingelaar, M. P. A. Geers, J. L. Duarte and M. A. M. Hendrix, *CO-tolerant operation of platinum-loaded PEM fuel cells*, Ieee, New York, 2007.

198. Z. Q. Mao, Y. J. Zhen, L. Y. Liu and W. Q. Lu, *Hydrogen Energy Progress XIII*, 2000, **2**, 863-866.

199. H. Lu, L. Rihko-Struckmann, R. Hanke-Rauschenbach and K. Sundmacher, *Top Catal*, 2008, **51**, 89-97.

200. P. P. Lopes, K. S. Freitas and E. A. Ticianelli, *Electrocatal*, 2010, **1**, 200-212.

201. O. A. Petrii, *J Solid State Electrochem*, 2008, **12**, 609-642.

202. A. Al-Ahmed, in *Current Application of Polymers and Nano Materials*, Trans Tech Publications Ltd, 2010.

203. T. C. M. Nepel, P. P. Lopes, V. A. Paganin and E. A. Ticianelli, *Electrochimica Acta*, 2013, **88**, 217-224.

204. M. Watanabe, *Journal of electroanalytical chemistry (1959)*, 1975, **60**, 267-273.

205. T. Maiyalagan and S. Pasupathi, *Materials Science Forum*, 2010, **657**, 143-189.

206. J.-H. Wee and K.-Y. Lee, *Journal of Power Sources*, 2006, **157**, 128-135.

207. B. Shabani, M. Hafttananian, S. Khamani, A. Ramiar and A. A. Ranjbar, *Journal of Power Sources*, 2019, **427**, 21-48.

208. X. Ren, Q. Lv, L. Liu, B. Liu, Y. Wang, A. Liu and G. Wu, *Sustainable Energy & Fuels*, 2020, DOI: 10.1039/C9SE00460B.

209. S. M. M. Ehteshami, Q. Jia, A. Halder, S. H. Chan and S. Mukerjee, *Electrochimica Acta*, 2013, **107**, 155-163.

210. Q. Wang, G. Wang, H. Tao, Z. Li and L. Han, *RSC Adv.*, 2017, **7**, 8453-8459.

211. R. Isseroff, L. Blackburn, J. Kang, H. Li, M. Gentleman and M. Rafailovich, *MRS Advances*, 2016, **1**, 1477-1486.

212. C. Wang, S. Wang, L. Peng, J. Zhang, Z. Shao, J. Huang, C. Sun, M. Ouyang and X. He, *Energies*, 2016, **9**, 603.

213. Q. Li, R. He, J. O. Jensen and N. J. Bjerrum, *Chemistry of Materials*, 2003, **15**, 4896-4915.

214. Y. Liu, Lehnert, W., Janßen, H., Samsun, R. C., Stolten, D., *Journal of Power Sources*, 2016, **311**, 91-102.

215. K. Sugiyama, Y. Sumiya, M. Takagi, K. Saita and S. Maeda, *Physical Chemistry Chemical Physics*, 2019, **21**, 14366-14375.

216. C.-H. Wan and Q.-H. Zhuang, *Electrochimica Acta*, 2007, **52**, 4111-4123.

217. J. Zhang, *PEM Fuel Cell Electrocatalysts and Catalyst Layers*, 2008.

218. T. Rajala, Master's Thesis, University of Helsinki, 2013.

219. M. Hafttananian, A. Ramiar and A. A. Ranjbar, *Energy Conversion and Management*, 2016, **122**, 564-579.

220. J. Scholta, J. Pawlik, N. Chmielewski and L. Jörissen, *Journal of Power Sources*, 2011, **196**, 5264-5271.

221. *U.S. Pat.*, 5,795,669, 1998.

222. S. Zhigang, Y. Baolian and H. Ming, *Journal of Power Sources*, 1999, **79**, 82-85.

223. R. W. Lindstrom, *Journal*, 1987.

224. A. Katsaounis, S. Balomenou, D. Tsiplakides, S. Brosda, S. Neophytides and C. G. Vayenas, *Applied Catalysis B: Environmental*, 2005, **56**, 251-258.

225. A. Katsaounis, S. P. Balomenou, D. Tsiplakides, M. Tsampas and C. G. Vayenas, *Electrochimica Acta*, 2005, **50**, 5132-5143.

226. J. Z. Zhang, Z. Liu and J. G. Goodwin, *Journal of Power Sources*, 2010, **195**, 3060-3068.

227. J. Z. Zhang, K. Hongsirikarn and J. G. Goodwin, *Journal of Power Sources*, 2011, **196**, 6186-6195.

228. C. Qin, J. Wang, D. Wang, B. Li and C. Zhang, *Catalysts*, 2016, **6**, 197.

229. A. Taniguchi, T. Akita, K. Yasuda and Y. Miyazaki, *Journal of Power Sources*, 2004, **130**, 42-49.

230. J. Saunders, B. Glenn, J. Myers, C. Cucksey, S. Mukerjee, C. Boggs and R. C. Urian, *ECS Transactions*, 2008, **6**, 343-349.

231. M. O. Ozdemir and U. Pasaogullari, *International Journal of Hydrogen Energy*, 2016, **41**, 10854-10869.

232. *U.S. Pat.*, 6,339,313 B1, 2002.

233. *U.S. Pat.*, 6,541,941 B2, 2003.

234. L. Palma, *IET Renewable Power Generation*, 2017, **11**, 314-319.

235. E4tech, U. E. Institute and K. Gastec, *Journal*, 2015.

236. G. Avgouropoulos, A. Paxinou and S. Neophytides, *International Journal of Hydrogen Energy*, 2014, **39**, 18103-18108.

237. T. Lopes, V. A. Paganin and E. R. Gonzalez, *International Journal of Hydrogen Energy*, 2011, **36**, 13703-13707.

238. S. Kaserer, C. Rakousky, J. Melke and C. Roth, *J Appl Electrochem*, 2013, **43**, 1069-1078.

239. G. Hinds and E. Brightman, *Electrochemistry Communications*, 2012, **17**, 26-29.

240. C. Quesada, T. Rockward, F. Garzon, D. Burleigh and R. Mukundan, *ECS Transactions*, 2014, **58**, 163-171.

241. Z. Noda, K. Hirata, A. Hayashi, T. Takahashi, N. Nakazato, K. Saigusa, A. Seo, K. Suzuki, S. Ariura, H. Shinkai and K. Sasaki, *International Journal of Hydrogen Energy*, 2017, **42**, 3281-3293.

242. C.-Y. Lee, C.-C. Chang and Y.-M. Lo, 2010, **10**, 10701-10713.

243. C. Y. Lee and C. W. Hsu, *Int. J. Electrochem. Sci.*, 2016, **11**, 2269-2275.

244. K. M. Caldwell, S. Kaserer, C. Roth and D. E. Ramaker, *ChemElectroChem*, 2015, **2**, 1502-1509.

245. G. Bender, M. Angelo, K. Bethune and R. Rocheleau, *Journal of Power Sources*, 2013, **228**, 159-169.

246. T. Bacquart, A. Murugan, M. Carré, B. Gozlan, F. Auprêtre, F. Haloua and T. A. Aarhaug, *International Journal of Hydrogen Energy*, 2018, **43**, 11872-11883.

247. D. Y. Chung, H. I. Kim, Y. H. Chung, M. J. Lee, S. J. Yoo, A. D. Bokare, W. Choi and Y. E. Sung, *Sci Rep*, 2014, **4**, 7450.

/